

**DEVELOPMENT OF ADVANCED CONTROL STRATEGIES FOR HIGH
PERFORMANCE SHAKE TABLE TESTS**

by

Jian-Yuan Lin

B.S. in Engineering, National Taiwan University, 2013

A THESIS SUBMITTED IN PARTIAL FULFILLMENT OF
THE REQUIREMENTS FOR THE DEGREE OF

MASTER OF APPLIED SCIENCE

in

THE FACULTY OF GRADUATE AND POSTDOCTORAL STUDIES
(Civil Engineering)

THE UNIVERSITY OF BRITISH COLUMBIA

(Vancouver)

April 2017

© Jian-Yuan Lin, 2017

Abstract

Shake table test provides a feasible solution for evaluating structural performances in earthquake engineering. It can test structural system in real time. However, high fidelity shake table control remains a challenging issue due to several difficulties, such as hydraulic actuator nonlinearity and the control-structure interaction (CSI) effect. Conventional shake table control employs linear controllers such as proportional-integral-derivative (PID) or loop-shaping controller to regulate the actuator's movement. However, it is difficult to tune a linear controller to accurately regulate the shake table when the payload and the hydraulic system are nonlinear. These challenges become more problematic when the payload mass is large relative to that of the table. Moreover, it is difficult to track a high frequency reference signal using a linear controller.

The main objectives of this study are to illustrate the implementation of hierarchical control and to improve the performance and robustness of shake table test. This thesis consists of three parts. First, the system identification procedure was used to investigate the dynamic characteristics of a hydraulic shake table at the University of British Columbia. The results of the system identification were used to build a reliable simulation model of the hydraulic shake table system. Second, the developed system identification model was used to develop different low-level controllers to regulate the actuator's movement. Third, advanced high-level control algorithms were implemented to increase tracking performance and control robustness. One nonlinear control algorithm named sliding mode control (SMC) and another optimal control algorithm named model predictive control (MPC) were presented in this thesis. The performance of the newly developed controllers was compared to that of the state-of-the-art linear controllers. The results show that the newly proposed hierarchical control architecture and the advanced high-level controller developed in this thesis can improve the tracking performance and robustness of shake table test.

Preface

Parts of the work in Chapter 2, 4 and 5 of this thesis have been accepted in the following peer reviewed conference proceeding and journal.

- Chapter 2: Yang, T. Y., Li, K., **Lin, J. Y.**, and Li, Y. (2013). “Development of Nonlinear Control Algorithms for Shaking Table Tests”, Proceedings, ASME Dynamic System and Control Conference, San Francisco, U.S, 2013.
- Chapter 4: Yang, T. Y., Li, K., **Lin, J. Y.**, Li, Y. and Zhang, Y. (2013). “Implementation of Nonlinear Control Algorithm for Shaking Table Tests”, Proceedings, 5th International Conference on Advances in Experimental Structure Engineering, Taipei, Taiwan, 2013.
Yang, T. Y., Li, K., **Lin, J. Y.**, Li, Y., and Tung, D. P. (2015). “Development of High-Performance Shake Tables Using the Hierarchical Control Strategy and Nonlinear Control Techniques.” *Earthquake Engineering & Structural Dynamics*, 44(11), 1717-1728.
- Chapter 5: Yang, T. Y., Li, K., **Lin, J. Y.**, Li, Y., and Tung, D. P. (2017). “Model Predictive Control Strategy in Shake Table Test”, Proceedings, 16th World Conference on Earthquake Engineering, Santiago, Chile, Jan. 9~13, 2017.

The author of this thesis is responsible for the literature review, controller design, simulation result and experiment implementation. The manuscripts were drafted by the author of the thesis and revised based on the comments from Prof. Tony Yang from University of British Columbia and Prof. Kang Li from National Taiwan University.

Table of Contents

Abstract.....	ii
Preface.....	iii
Table of Contents	iv
List of Tables	vii
List of Figures.....	viii
List of Abbreviations	x
List of Symbols	xi
Acknowledgements	xv
Dedication	xvi
Chapter 1: Introduction	1
1.1 Overview.....	1
1.2 Literature Review.....	2
1.2.1 Proportional-Integral-Differential (PID) Control	3
1.2.2 Three-Variable-Control.....	4
1.2.3 Iterative Control Method.....	4
1.2.4 Other Control Schemes	7
1.3 Hierarchical Control Framework	8
1.4 Thesis Scope	9
1.5 Organization of Thesis	10
Chapter 2: System Identification for Shake Table System	12
2.1 Overview.....	12

2.2	Hydraulic System Dynamics.....	14
2.2.1	Concept.....	14
2.2.2	Physical Equations.....	15
2.3	System Identification Method.....	18
2.3.1	Experimental Setup.....	18
2.3.2	System Identification for Hydraulic Actuator.....	20
2.3.3	System Identification for Shake Table.....	25
2.4	Summary.....	29
Chapter 3: Low-level Controller Design.....		31
3.1	Overview.....	31
3.2	PID Control.....	31
3.2.1	Theory.....	31
3.2.2	PID Controller Design.....	33
3.3	Three Variable Control.....	36
3.4	Loop-shaping Control.....	38
3.5	Summary.....	41
Chapter 4: Sliding Mode Control.....		42
4.1	Theory Background.....	42
4.2	Control Law Derivation.....	45
4.3	Implementation.....	49
4.4	Experiment Result.....	50
4.5	Summary.....	54
Chapter 5: Model Predictive Control.....		56

5.1	Overview.....	56
5.2	Theory.....	58
5.3	Controller Design.....	61
5.3.1	Prediction Model Design	61
5.3.2	State Estimation and Prediction.....	65
5.3.3	Optimization	66
5.4	Simulation Result.....	68
5.5	Comparison between SMC	72
5.6	Summary.....	74
Chapter 6: Summary and Conclusion.....		75
6.1	Conclusion	75
6.2	Future Work	78
Bibliography		80
Appendices.....		83
	Appendix A Simulation specimen design.....	83

List of Tables

Table 3-1 PID control gain effect	32
Table 3-2 Gain setup for TVC	37
Table 4-1 Acceleration tracking error analysis in time and frequency domains	54
Table 5-1 MPC parameters setup.....	68
Table 5-2 Acceleration tracking comparison for MPC and SMC.....	73

List of Figures

Figure 1-1 PID feedback control structure.....	3
Figure 1-2 Hydraulic shake table control system scheme	5
Figure 1-3 Block diagram of the acceleration trajectory tracking controller.....	7
Figure 1-4 Dual loop control architecture.....	8
Figure 1-5 Hierarchical control framework	9
Figure 2-1 Basic hydraulic system structure (credits to Jelali and Kroll 2012).....	14
Figure 2-2 Model structure for hydraulic actuator and shake table system.....	17
Figure 2-3 Experimental setup in UBC	19
Figure 2-4 Equivalent mass on the shake table.....	19
Figure 2-5 Subspace system identification flow chart.....	22
Figure 2-6 Input and output data for hydraulic actuator model.....	24
Figure 2-7 Simulation model fit for hydraulic actuator	24
Figure 2-8 Transfer function parameters estimation procedure.....	25
Figure 2-9 Input and output data for shake table model	28
Figure 2-10 Measured and simulated model output for shake table model.....	29
Figure 3-1 PID control block diagram.....	32
Figure 3-2 PID control in hydraulic shake table system.....	33
Figure 3-3 Displacement PID controller design	35
Figure 3-4 Force PID controller design	35
Figure 3-5 Control structure for proposed TVC	36
Figure 3-6 Time domain comparison for TVC and PID control	37
Figure 3-7 Frequency domain comparison for TVC and PID control.....	38

Figure 3-8 Loop-shaping control block diagram	38
Figure 3-9 Loop-shaping controller design.....	40
Figure 3-10 Close-loop response comparison between PID and loop-shaping controller.....	40
Figure 4-1 Lyapunov theory example: nonlinear mass spring damper system	43
Figure 4-2 Schematic plot of the SDOF shake table model.....	45
Figure 4-3 Implementation of the hierarchical control architecture of the shake table test	50
Figure 4-4 Comparison of the table performances	52
Figure 4-5 Photos of the damaged specimen	53
Figure 4-6 Specimen hysteresis	53
Figure 5-1 MPC schematic	59
Figure 5-2 MPC structure	60
Figure 5-3 Prediction model architecture for MPC	62
Figure 5-4 Process model block diagram.....	62
Figure 5-5 Comparison result for shake table without specimen	70
Figure 5-6 Comparison result for shake table with specimen.....	72
Figure A-1 Schematic Diagram of the SDOF Shake Table Model	83

List of Abbreviations

CSI: control-structure interaction

PID: proportional-integral-differential

TVC: three-variable-control

FFT: fast fourier transform

SMC: sliding mode control

MPC: model predictive control

MIL: model-in-the-loop

SVD: singular value decomposition

LVDT: linear variable differential transformer

SDOF: single degree of freedom

LQR: linear-quadratic regulator

LQG: linear-quadratic-Gaussian

QP: quadratic programming

RHC: receding horizon control

MSSC: multiple sliding surface control

DSC: dynamic surface control

RHSC: receding horizon sliding control

List of Symbols

k_q : the linearized flow gain

k_c : the leakage constant

β : the bulk modulus of hydraulic fluid

O_r : the extended observability matrix

α_k : the step length in Gauss Newton method

p_k : the search direction in Gauss Newton method

$r(\theta)$: the residual vector in Gauss Newton method

$J(\theta)$: the Jacobian matrix in Gauss Newton method

k_p : the proportional gain in PID control

k_I : the integral gain in PID control

k_D : the derivative gain in PID control

r : the displacement reference signal

\dot{r} : the velocity reference signal

\ddot{r} : the acceleration reference signal

x : the measured displacement signal

\dot{x} : the measured velocity signal

\ddot{x} : the measured acceleration signal

K_{bd} : the displacement feedback gain in TVC

K_{bv} : the velocity feedback gain in TVC

K_{ba} : the acceleration feedback gain in TVC

K_{fd} : the displacement feedforward gain in TVC

K_{fv} : the velocity feedforward gain in TVC

K_{fa} : the acceleration feedforward gain in TVC

$L(s)$: the loop function in Loop-shaping control

m_t : the table mass in the SDOF shake table model

m_s : the specimen lump mass in the SDOF shake table model

d_t : the relative displacement of the table with respect to the ground

d_s : the relative displacement at the top of the specimen with respect to the table

\dot{d}_s : the relative velocity of the specimen

\ddot{d}_t : the acceleration of the shake table

\ddot{d}_s : the relative acceleration of the specimen

k : the external spring stiffness in the shake table system

P_s : the specimen resisting force

F : the applied force to shake table system

S : the sliding surface

\tilde{x}_1 : the displacement tracking error in SMC

$\dot{\tilde{x}}_1$: the velocity tracking error in SMC

x_1 : the actual displacement in SMC

x_{1d} : the desired displacement in SMC

\dot{x}_1 : the actual velocity in SMC

\dot{x}_{1d} : the desired velocity in SMC

λ : the tuning parameter for the ratio between displacement and velocity tracking error in SMC

K : the tuning parameter for the convergence rate in SMC

F_{disp} : the displacement command from SMC

$F_{v/a}$: the force command from SMC

M : the priori estimate error covariance in Kalman Filter

Q : the process noise covariance matrix in Kalman Filter

R : the measurement noise covariance matrix in Kalman Filter

p : the prediction horizon

u_{disp} : the control signal from MPC to the displacement loop in TVC

u_{vel} : the control signal from MPC to the velocity loop in TVC

u_{acc} : the control signal from MPC to the acceleration loop in TVC

w_{disp} : the weighting for displacement control loop

w_{vel} : the weighting for velocity control loop

w_{acc} : the weighting for acceleration control loop

r_{disp} : the reference input for displacement loop

r_{vel} : the reference input for velocity loop

r_{acc} : the reference input for acceleration loop

y_{disp} : the predicted displacement from the Kalman Filter

y_{vel} : the predicted velocity from the Kalman filter

y_{acc} : the predicted acceleration from the Kalman filter

$w_{\Delta disp}$: the weighting for displacement input change rate

$w_{\Delta vel}$: the weighting for velocity input change rate

$w_{\Delta acc}$: the weighting for acceleration input change rate

ρ_ε : the weighting for constraint violation

ε_k : the slack variable for constraint softening

Acknowledgements

I would like to give my special thanks and gratitude to my supervisor, Prof. Tony Yang. Through the past two and half years, his intelligence, patience, passion and diligence to research have set up a great role model for me to follow. It has been a great honor and pleasure to work under his guidance, and I look forward to the future collaborations with him. Furthermore, I would like to thank my second supervisor, Prof. Kang Li in National Taiwan University. Thanks for guiding me through the past years beginning from my undergraduate studies and the professional training is extremely useful after I step into the graduate study field.

I would like to thank Mr. Dorian Tung and Mr. Yuanjie Li for working with me on different exciting projects in the structure laboratory and except for helping me in academic, they are always willing to give me their own opinions on my future career. Many thanks also belong to my other research colleagues, Lisa Tobber and Jeremy Atkinson for their valuable help in my research and life. I also want to convey my sincere gratitude to many people in Taiwanese Graduate Student Association (TGSA) including Sue-Jin Lin, Ting-Chun Kuo, Tse-Hua Chao, Yu-Ling Chuang and Wei-Chung Chen, for their kind help when I first arrived in Vancouver. The research presented in this thesis also owes many thanks to Scott Jackson, Harald Schremp and Bill Leung for their assistance in the structural lab. Special thanks will go to my closest friends Tzu-Hsien Shih, Jordan Karyanto and Xu Xie for their genuine friendship through these two and half years in Vancouver.

Lastly, I would like to express my deepest gratitude for my family's unconditional love, continuous support for my education and their useful advice when I faced different challenges. Without their support, I can't achieve anything in my graduate study career.

Dedication

To my family for their unconditional love and support

Chapter 1: Introduction

1.1 Overview

Shake table test is a state-of-the-art experimental method used to evaluate structural performance in earthquake engineering. It can provide base excitation and examine structural behavior under extreme conditions, which allows researchers and engineers to investigate structure performance and validate its proposed design. The goal of shake table control is to reproduce selected time history data, which is typically an acceleration trajectory. With the development of technology in terms of sensors and actuators, the hardware setup and the testing capacity of the shake table has evolved significantly. However, technical issues have been raised up in shake table control concerning its complexity and nonlinearity. The hydraulic shake table system is usually composed of the hydraulic actuator, shake table and test specimen. The hydraulic actuator itself is a highly nonlinear system, which means that under different operating points, its dynamics can vary considerably. Moreover, the payload on the shake table also changes the hydraulic actuator dynamics, especially when nonlinear behavior occurs in the specimen. Therefore, the hydraulic shake table control issue can be regarded as a highly nonlinear control problem, with good acceleration tracking continuing to pose a challenge.

To solve the control problem in the hydraulic shake table system, this thesis proposes a novel control architecture known as the hierarchical control framework. The hierarchical control system is a form of control system in which a set of devices and governing algorithms is arranged in a hierarchical tree. The architecture consists of a high-level controller along with one or more

low-level controller(s). The high-level controller, which takes into account the shake table system dynamics, is designed to control table movement so as to track the desired reference signal and guarantee global system stability, while the low-level controller(s) are used to regulate the output response of the actuator according to the commands generated by the high-level controller. The main advantage of the hierarchical control approach is it can separate and simplify complex system control problems into two levels of control tasks to be executed by the high-level and low-level controllers, respectively. The high-level controller governs shake table motion and handles the overall control system's stability and reference signal-tracking requirements. On the other hand, the low-level controller functions as the actuator controller and simply regulates the actuator output to follow commands from the high-level controller.

In this thesis, the hierarchical control framework, including the low-level and high-level controller designs, is demonstrated to solve the shake table control problem. The results reveal that the proposed strategy outperforms the traditional linear control in the tracking results and provides a feasible solution to the shake table control problem.

1.2 Literature Review

The development of the shake table can be traced back to the first hand-powered table created in the 19th century (Severn 2011). Through the years, the specification and functionality of the modern shake tables have greatly improved. In the past twenty years, high performance shake tables such as the large outdoor shake table at the University of California, San Diego, the E-Defense shake table in Japan, and the multi-function shake table array at the Tongji University in China have been successfully constructed.

Although testing capacity and hardware quality have been greatly improved, high fidelity shake table control remains a challenging issue. The purpose of the shake table control systems is

to reproduce the reference input signal within a range of reasonable accuracy. Due to several difficulties, such as the inherent hydraulic actuator's nonlinearity and control-structure interaction (CSI) effects (Dyke *et al.* 1995), achieving perfect tracking for the specimens on the shake table remains a challenging issue. The above challenges become even more problematic when the specimen exhibits nonlinear behaviour and when its mass is large relative to that of the table (Phillips *et al.* 2014). Tremendous work has been done to improve the shake table test's control performance. The following sections summarize the development of the control strategy in the hydraulic actuator and shake table control.

1.2.1 Proportional-Integral-Differential (PID) Control

Proportional-Integral-Differential (PID) control is the most common industrial application (Bennett 1993). The control scheme is depicted in Figure 1-1. The input is the reference signal to be tracked, while the output is the physical measurable movement in the shake table. Feedback is obtained through the pre-installed sensor. The error term is the difference between the reference input and the measured output.

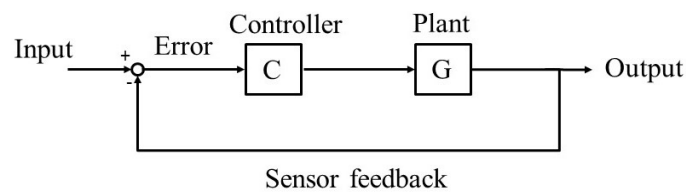


Figure 1-1 PID feedback control structure

PID control utilizes proportional, integral and differential gain to minimize the error term and achieve the tracking purpose. In hydraulic shaking table applications, the feedback usually is chosen as a displacement due to the stability issue. Under common scenario, PID controller can stabilize the system and achieve certain tracking performance. However, the PID controller is unable to achieve the requirements of earthquake engineering, including wide control bandwidth

and high tracking performance. Therefore, the following control technique has been developed to improve the performance.

1.2.2 Three-Variable-Control

To improve the control bandwidth, the three-variable-control (TVC) was developed and has been successfully implemented in hydraulic shaking tables (Tagawa and Kajiwara 2007; Nowak et al. 2000). The three variables in the TVC represent the displacement, velocity and acceleration of the shake table. TVC can extend the system's frequency bandwidth and improve its stability; it is usually employed for acceleration control. The TVC can be separated into feedback and feedforward portions. In the feedback segment, there are three feedback loops, i.e. the displacement, velocity and acceleration feedback loops with three gains, respectively. There are also three gains in the feedforward portion in TVC, respectively. The feedback segment is responsible for robustness and the stability issue, while reference tracking performance is improved by adjusting the feedforward gains. By utilizing the six parameters in the TVC, it is feasible to manually tune a parameter set onsite. However, since the shake table and specimen form a nonlinear system and it is expected that the shake table's dynamics will be influenced by the specimen, one parameter set might not be a universal solution for all scenarios.

1.2.3 Iterative Control Method

Since the shake table is coupled with the pre-installed specimen, the specimen is expected to influence the shake table's dynamics, and the traditional control techniques including PID control and TVC are not expected to provide a universal solution to this control problem. Therefore, the iterative control method (Tagawa and Kajiwara 2007) is employed to compensate for control performance. Were one to consider the entire shake table system, including the controller, shake table, hydraulic actuator and specimen, as a single dynamic system, then the input

for this system would be the acceleration reference data, while the output would be the measured acceleration (Yao et al. 2014). Figure 1-2 shows the iterative control scheme. Since $G(\omega)$ contains the dynamics of the controller, hydraulic actuator, shake table and specimen, $G(\omega)$ is a highly nonlinear system.

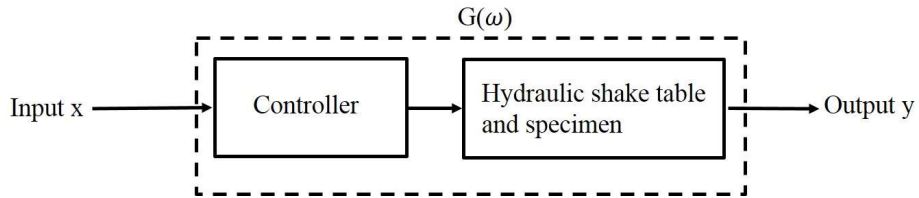


Figure 1-2 Hydraulic shake table control system scheme

The iterative control is essentially an offline feedforward method. First, a random reference acceleration input signal is implemented into the hydraulic shake table control system. The frequency response of the entire control system, i.e. $G(\omega)$, can be calculated using the fast fourier transform (FFT) and presented in Equation 1-1.

$$Y(\omega) = G(\omega)X(\omega) \quad \text{Equation 1-1}$$

where $X(\omega)$ and $Y(\omega)$ are the FFT results of x and y , respectively. $G(\omega)$ is the frequency response model of the hydraulic shake table system.

It can be assumed that, for a given earthquake acceleration input $X_e(\omega)$, the following relationship can be obtained in Equation 1-2:

$$Y_e(\omega) = G_e(\omega)X_e(\omega) \quad \text{Equation 1-2}$$

where $G_e(\omega)$ and $Y_e(\omega)$ are the frequency response and output of the hydraulic shake table system for a given input $X_e(\omega)$, respectively.

If the system is linear, $G_e(\omega)$ must be equal $G(\omega)$ and thus Equation 1-3 can be obtained. By using an inverse calculation, the relationship between the modified reference input and desired output can be obtained as Equation 1-4.

$$Y_e(\omega) = G(\omega)X_e(\omega) \quad \text{Equation 1-3}$$

$$X_d(\omega) = G(\omega)^{-1}Y_d(\omega) \quad \text{Equation 1-4}$$

where $X_d(\omega)$ is the modified reference input and $Y_d(\omega)$ is the desired output, which means the desired acceleration feedback on the shake table.

The goal of the shake table test is to reproduce the reference acceleration signal on the shake table. It can be observed that the desired output, $Y_d(\omega)$, can be realized by implementing the modified reference input, $X_d(\omega)$, and the relationship is presented in Equation 1-5.

$$\begin{aligned} Y_e(\omega) &= G(\omega)X_e(\omega) = G(\omega)X_d(\omega) \\ &= G(\omega)G(\omega)^{-1}Y_d(\omega) = Y_d(\omega) \end{aligned} \quad \text{Equation 1-5}$$

However, the system is highly nonlinear in the real laboratory. This means that the frequency response model in Equation 1-1 is different from the model in Equation 1-2. By separating the model into nominal and modelling error parts, Equation 1-2 can be rewritten as the following Equation 1-6. By repeating the above procedure, a similar equation can be obtained as Equation 1-7.

$$Y_e(\omega) = [G(\omega) + \bar{G}(\omega)]X_e(\omega) \quad \text{Equation 1-6}$$

$$Y_e(\omega) = [1 + \bar{G}(\omega)G(\omega)^{-1}]Y_d(\omega) \quad \text{Equation 1-7}$$

where $\bar{G}(\omega)$ is the modelling error part.

It can be observed that an error term appears; to minimize this error, the user needs to tune the modified reference input iteratively to reduce the tracking error. The main problem in the iterative control method is that it requires many trials, meaning many shake table tests, to eliminate the error term and achieve acceptable tracking performance. The specimen can be damaged or even collapse through the iterations. The other problem is that if the specimen is highly nonlinear, the convergence of the iterative control method is not guaranteed.

1.2.4 Other Control Schemes

Nakata (2010) developed an acceleration trajectory tracking control method to improve the acceleration tracking ability of the shake table. The method consists of an acceleration feed-forward, a system dynamics command shaping, an intentional time-delay, a Kalman filter to reduce the degree of noise in the measured actuator displacement, and an actuator displacement feedback to ensure stability. It was experimentally demonstrated that this approach improved tracking performance over the conventional displacement feedback controllers with command shaping. A block diagram for this method is shown in Figure 1-3. However, its payload contribution is not included in this framework. This scheme is highly dependent on the system's dynamics, which can be altered by the payload effect.

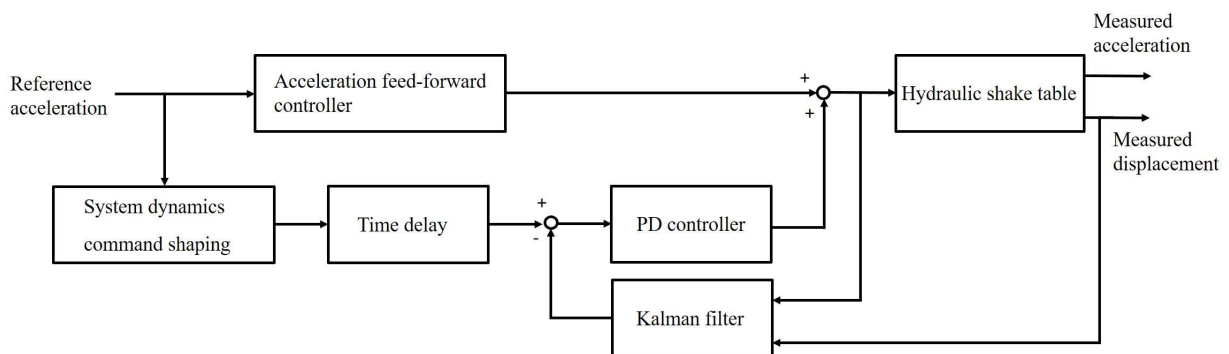


Figure 1-3 Block diagram of the acceleration trajectory tracking controller

Stehman and Nakata (2013) proposed a different acceleration control strategy using a dual control loop. It consisted of an acceleration feedback control loop to track acceleration and a force feedback control loop to prevent table drift. Possessing a pre-gain for each controller, the final command to the actuator was the sum of the commands from both control loops. When compared with a conventional displacement-based PID controller, the approach had improved acceleration tracking performance and was demonstrated using experimental data in both the time and frequency domains. The dual loop control's architecture is shown in Figure 1-4. However, this technique still utilized linear controller and its performance is not guaranteed when the specimen is nonlinear.

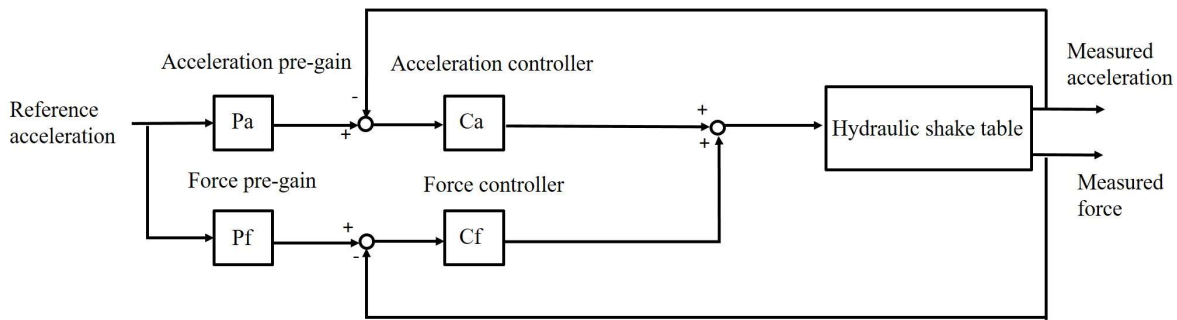


Figure 1-4 Dual loop control architecture

1.3 Hierarchical Control Framework

Divergent from the previously mentioned control scheme, a novel control structure termed hierarchical control is developed in this thesis. It consists of a high-level nonlinear controller deployed for tracking a desired reference signal, and a low-level controller for actuator control. The hierarchical control framework is shown in Figure 1-5. The low-level controller takes its commands from the high-level one to regulate the actuator's output through feedback control. The

high-level controller governs the system's overall tracking performance and deals with nonlinearities in the hydraulic actuator and shake table system.

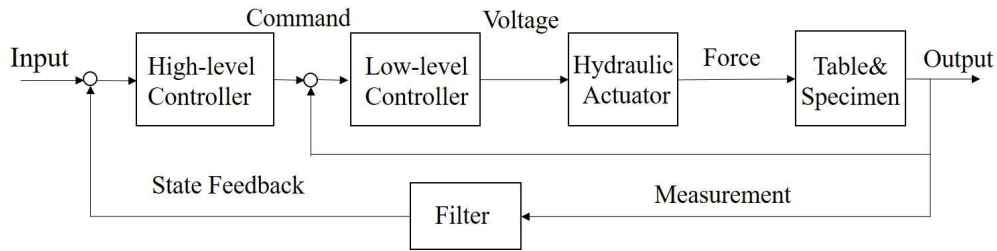


Figure 1-5 Hierarchical control framework

A system identification procedure is applied to capture the system dynamics of the hydraulic actuator. The low-level controller is designed to regulate the hydraulic actuator based on the simulation model that is generated from the system identification process. For the high-level controller, two advanced control strategies are presented in this thesis. One is a nonlinear controller termed a sliding mode control (SMC), while the other one is a model-based optimal controller labelled a model predictive control (MPC). The advantage of the SMC is that it can provide robustness against nonlinearities in both the shake table dynamics and the specimen's behaviour, while achieving good tracking performance despite the nonlinearities in the specimen. The MPC was investigated in the simulation mode; it subsequently displayed high quality tracking performance and the potential to outperform the existing linear controller in the laboratory.

1.4 Thesis Scope

Three main objectives are presented in this thesis. The first is to introduce the hierarchical control framework and its advantage for the shake table control system. Traditional shake table controls utilize linear control and only have one controller to handle both trajectory tracking and actuator movement, which is difficult for one linear controller to handle. The hierarchical control

framework separates the task into two levels, making it more feasible for solving the control problems extant in each layer.

The second objective of the thesis is to introduce the concept of model-in-the-loop (MIL) simulation. Following this method, the system identification for the hydraulic actuator and shake table systems is performed, following which the precise simulation models are built. By constructing this simulation framework, the controller design and parameter tuning can be conducted in simulation rather than by using the actual hardware.

The third intent is to present the advanced control algorithm design in the shake table test. Two control algorithms were chosen for demonstration. One is a nonlinear control algorithm termed the sliding mode control (SMC), while the other is an optimization control algorithm designated the model predictive control (MPC). Both controller designs possess the potential to replace the tradition linear control, proving the advantage of the hierarchical control framework.

1.5 Organization of Thesis

The hierarchical control framework, system identification, and low-level and high-level controller designs, with the high-level including the sliding mode and model predictive controls are presented in this thesis.

Chapter 2 comprises a detailed explanation of the system identification for the hydraulic actuator and shake table system. The physical equations of the hydraulic system are listed and the CSI effect discussed. Subsequently, the subspace system identification method is utilized to generate the precise simulation model for the hydraulic actuator, while the Gaussian Newton method (Nocedal and Wright 1999) is employed to ascertain a simulation model for the shake table. The simulation framework provides a reliable solution for controller tuning and design.

Chapter 3 describes the low-level controller design based on the simulation model constructed in Chapter 2. The traditional PID controller, TVC and loop-shaping controller design are presented. The controller parameter tuning is performed in a simulated environment as opposed to the real hardware environment. This method is called MIL simulation, and has the potential for saving much expense and time, since the traditional means for controller tuning has been to change the parameters iteratively in real-time.

Chapter 4 presents a high-level controller design using a nonlinear control algorithm termed a sliding mode control (SMC). This controller design method utilizes the Lyapunov theorem and provides robust performance in dealing with system uncertainties and specimen nonlinearities. A comparison between the SMC and traditional linear controller is done. The experiment results reveal that the SMC outperformed the traditional linear controller in terms of tracking performance and system robustness.

Chapter 5 presents another high-level controller design using an optimization based strategy known as model predictive control (MPC). This controller design requires the employment of a precise model in a low-level control process, and then calculates the optimal control command based on the low-level system dynamics. Simulation results illustrate that the MPC has the potential to achieve high performance acceleration tracking results.

Chapter 6 provides a summary for the research findings, conclusions and recommendations for future work and research.

Chapter 2: System Identification for Shake Table

System

2.1 Overview

Shake table testing is performed with the hydraulic servo system to provide base excitation to the structures under test. Its control algorithm design requires dynamic models of the structure as well as the hydraulic actuators, which both can potentially be highly nonlinear. Since the dynamic models and parameters of hydraulic systems are generally unknown to the users of their control systems, users can usually only blindly tune the parameters of actuator controllers via trial and error. However, the performance and stability of such controllers is not guaranteed and is unpredictable, since the actual operating points of the hydraulic system dynamics during the generally nonlinear experimental process can significantly deviate from the operating point at which the controller is tuned. Therefore, the system identification procedure needs to be performed prior to the controller design phase.

Traditional system identification can be categorized into three methods (Ljung 1999). The first is the white box method, which involves constructing the model based on the known governing equations and parameters of the system. This approach is also called the physical modeling method. This method would be ideal except that it is generally impractical to obtain all the necessary parameters of the actual physical system. The second method is the black box, which is aimed at building a model for an unknown system based on experimental input and output data

without prior knowledge of the system's design or detailed parameters. This method is usually more feasible for users of the hydraulic system to operate, and is less time-consuming since it does not require any background knowledge of the hydraulic system. However, the potential problem with this approach is that the obtained model cannot fully describe the dynamics of the system within its operating range if the system identification experiments are not conducted properly. The third approach is known as the grey box method, in which the model of the system is constructed based on a partial knowledge of the physical system model and experimental data. The experimental data are used to provide an estimation of the unknown parameters and subsystems of the system's incomplete physical model. This approach is also labelled the semi-physical modeling method, since it combines physical insight with actual experiment data.

In this chapter, the grey box modeling method for the hydraulic actuator and shake table is presented and the simulation model constructed for controller design purpose. The physical equations are discussed to demonstrate the preliminary insight into the hydraulic system, and experimental data is then collected to construct the entire model. The subspace system identification method is chosen to compute the state space model for the hydraulic system. The model for the shake table dynamics is also constructed using the same method. The entire model structure is presented to show the effects of the control structure interaction (CSI). In the end, the simulation and experimental results are compared to show the reliability and accuracy of the constructed simulation model.

2.2 Hydraulic System Dynamics

2.2.1 Concept

The hydraulic servo system can be considered an arrangement of individual components, interconnected to provide the desired form of hydraulic transfer (Jelali and Kroll 2012). Figure 2-1 shows the basic hydraulic system's structure, which consists of the following three levels:

1. Power supply (pump, accumulator, cooler, filter...)
2. Control elements (valve, sensor, controller...)
3. Actuating elements (cylinder and/or motor)

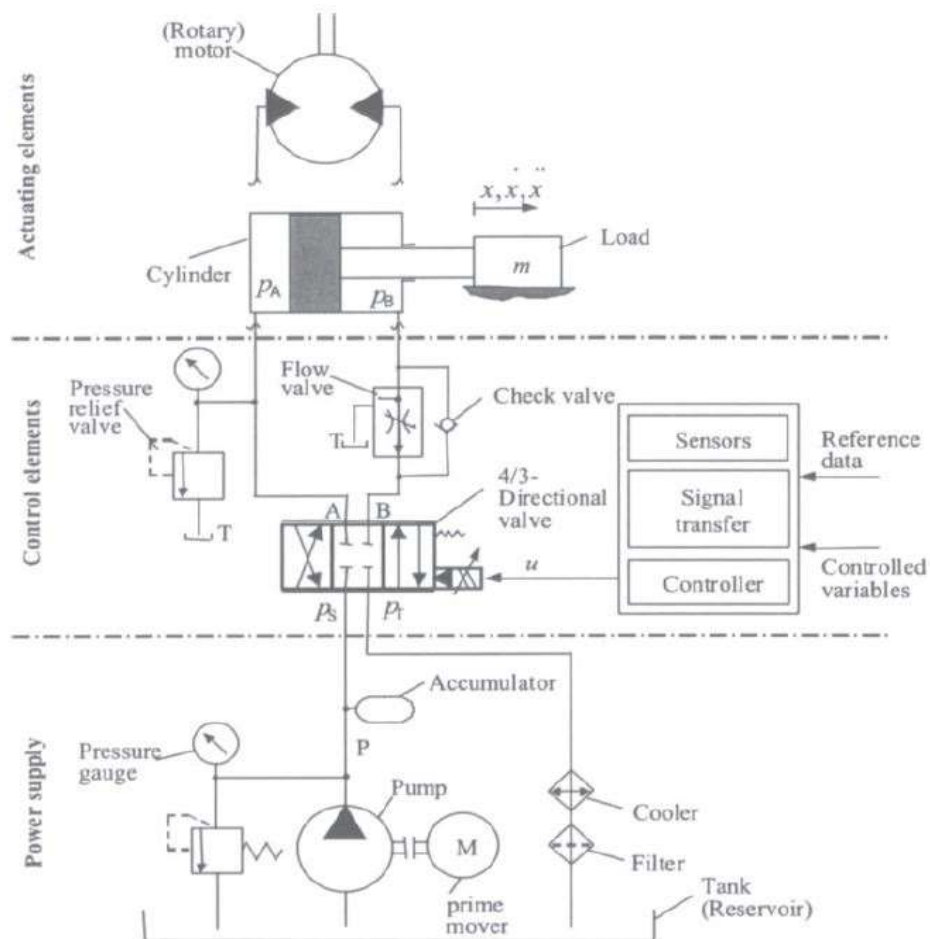


Figure 2-1 Basic hydraulic system structure (credits to Jelali and Kroll 2012)

The standard valve-controlled hydraulic system is used here as an example to briefly outline the physical operating concept of the hydraulic system. In the power supply stage, the pump converts mechanical power from the prime mover to hydraulic power at the actuator, and the fluid storage and conditioning equipment such as the filter, accumulator and cooler ensure the sufficient quality, quantity and cooling of the fluid. Valves are used to control the direction of pump flow, the level of the power produced, and the amount of fluid and pressure on the actuator. It should be noted that this is where the control algorithm comes in, since the valve is controlled by the voltage generated by the controller. A linear actuator (cylinder) or a rotary actuator (motor) converts the hydraulic power to usable mechanical power output at the point required. In the shake table application, the linear type actuator is used to implement movement.

2.2.2 Physical Equations

The physical equations for the hydraulic system are presented in this section and might provide some insight to facilitate the construction of the model from the experimental data. It should be noted that this depends on the type of hydraulic actuator employed, since the individual components might differ slightly, negating the possibility for creating a universal model for the hydraulic actuator.

The input signal into hydraulic actuator system is the valve command generated by the controller, which is usually a direct current voltage signal. The linearized relationship between the oil flow, valve command and leakage can be represented in Equation 2-1 (Ozcelik 2008).

$$q = k_q u - k_c \frac{f}{A} \quad \text{Equation 2-1}$$

where u is the valve command, k_q is the linearized flow gain, k_c is the leakage constant, f is the actuator force and A is the effective actuator piston area.

From the flow continuity equation, the flow can also be represented in Equation 2-2.

$$q = A\dot{x} + \frac{V}{2\beta A} \dot{f} \quad \text{Equation 2-2}$$

where \dot{x} is the velocity of the actuator piston, V is the hydraulic fluid volume for the actuator, and β is the bulk modulus of hydraulic fluid.

Equating Equation 2-1 and Equation 2-2 and take Laplace transformation, the relationship between valve command, velocity of the actuator piston and the actuator force can be represented as Equation 2-3.

$$k_q u - A\dot{x} = \left(\frac{k_c}{A} + \frac{Vs}{2\beta A} \right) f \quad \text{Equation 2-3}$$

where s is the Laplace variable.

By rearranging Equation 2-3, a simple relationship to represent the hydraulic actuator system can be formulated as Equation 2-4.

$$f = G_1(s)u + G_2(s)\dot{x} \quad \text{Equation 2-4}$$

where $G_1(s) = \frac{2\beta Ak_q}{2\beta k_c + Vs}$ and $G_2(s) = \frac{-2\beta A^2}{2\beta k_c + Vs}$.

This equation implies that the actuator force is related to two inputs. The first is the voltage command and the second the actuator piston velocity, which is the so-called control-structure interaction (CSI) (Dyke *et al.* 1995). As mentioned in the previous discussion, the physical equations might alter from one actuator to the other, with a lack of universality between the coefficients and order of the transfer function. However, from the physical equations, the hydraulic actuator can be defined as a model with two inputs, the voltage and piston velocity, and a single output, the actuator force. The model's parameters and order can be obtained from the experimental data by implementing the system identification algorithm.

It should be noted that since the actuator is attached to the shake table, the actuator piston's velocity should be equal to the velocity of the shake table. Therefore, a dynamic model for the shake table is also required to provide velocity feedback to the actuator model. A mass-spring-damper system can be used to describe the shake table's dynamics. The second order transfer function that applies the actuator force as input and the shake table displacement as output is represented in Equation 2-5. The parameters for the shake table model can also be ascertained using the system identification algorithm and experimental data. Figure 2-2 is the model structure for the hydraulic actuator and shake table system.

$$G_{table}(s) = \frac{1}{ms^2 + cs + k} x \quad \text{Equation 2-5}$$

where m is the table mass, and c and k are the damping coefficient and stiffness coefficients for the shake table system, respectively.

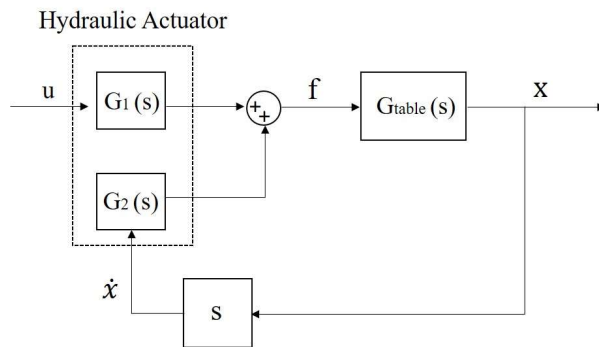


Figure 2-2 Model structure for hydraulic actuator and shake table system

From Equation 2-5 and Figure 2-2, it can be observed that the hydraulic actuator dynamics is influenced by the velocity feedback from the shake table. The main advantage of this model structure is that, once the actuator model is found (i.e. G_1 and G_2), the user can adjust the parameters of the shake table portion to simulate the CSI effect after incorporating the payload and

implement controller into the simulation mode. This method is called model-in-the-loop (MIL) simulation, and it can efficiently save costs since it does not involve any direct installations into real hardware.

2.3 System Identification Method

In the hydraulic shake table control application, two models can be identified from the experimental data. One is the hydraulic actuator model and the other the shake table model. From Figure 2-2 and the formula derivation in Section 2.2, the hydraulic actuator model takes voltage and velocity as input data and force as output data. For the shake table model, it takes force as input data and displacement as output data. The scope of the system identification problem is to find a numerical model to provide precise fitting results from the experimental input and output data. Section 2.3.1 outlines the experimental setup for the uniaxial shake table in the structure laboratory at the University of British Columbia. In the Section 2.3.2, the subspace system identification method is chosen to postulate a state-space model to represent the hydraulic actuator from the experimental data; this model is then converted to a transfer function model to match the framework presented in Figure 2-2. In Section 2.3.3, the second order linear transfer function in Equation 2-5 is chosen to fit the experimental data while the instrumental variable (IV) and Gauss-Newton methods are employed to ascertain the parameters.

2.3.1 Experimental Setup

A single degree of freedom shake table is constructed at the University of British Columbia (UBC) as shown in Figure 2-3. The linear variable differential transformer (LVDT) is employed to measure the displacement, and the load cell is installed to measure the actuator force applied by the MTS hydraulic actuator (Model Number 402.08). The actuator has a stroke of ± 1.5 inches and capacity of 1.1 kips. Since there is no velocity sensor, the velocity is estimated by differentiating

the displacement measurement. The accelerometer is installed on the shake table to measure the base acceleration. If the specimen is installed on the shake table, another accelerometer will be installed on the specimen to measure the top acceleration. The experimental data is collected using ACTS control software and an ACTS data acquisition device. To prevent the pre-damage of the specimen, the equivalent mass is placed on the shake table to implement the system identification test. The system identification setup is presented in Figure 2-4.

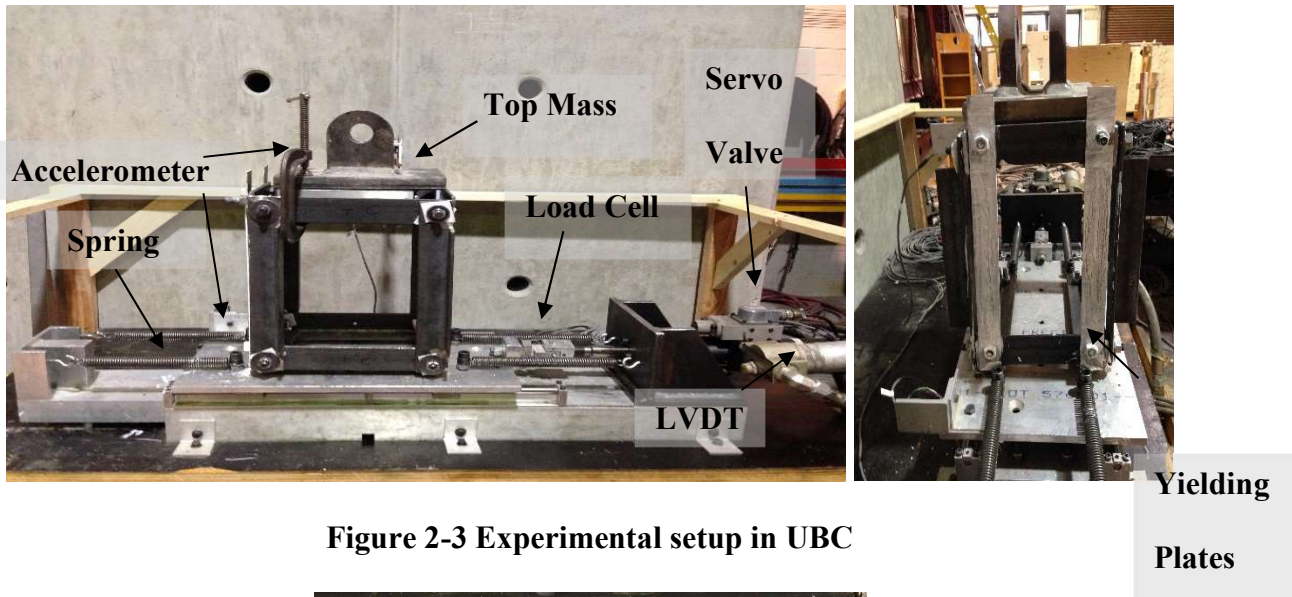


Figure 2-3 Experimental setup in UBC



Figure 2-4 Equivalent mass on the shake table

2.3.2 System Identification for Hydraulic Actuator

The subspace system identification method is chosen to build the state-space model for the hydraulic actuator. This does not require any iterative calculation and the numerical implementation is already proven to be reliable and well-developed. The method's general theory will be presented in this section.

A stochastic linear system can be formulated in the following state space form.

$$\begin{aligned}x(t+1) &= Ax(t) + Bu(t) \\y(t) &= Cx(t) + Du(t)\end{aligned}\tag{Equation 2-6}$$

where $x(t), u(t)$ and $y(t)$ are the system state, input and output, respectively. A, B, C and D are system matrices with appropriate dimensions.

A is called the dynamical system matrix. It describes the dynamics of the system; the eigenvalues of Matrix A will capture all the dynamical modes and govern the stability. B is the input matrix which represents the relationship that the deterministic inputs influence in the next state. C is the output matrix, which describes the transformation of the internal state to the system output. The term with Matrix D is known as the direct feedthrough term. In continuous time systems, this term is most often labelled "0". It should be noted that the state space representation is not unique. For any invertible matrix T , same input-output relationship can be described by changing the basis $\tilde{x}(t) = T^{-1}x(t)$.

$$\begin{aligned}\tilde{x}(t+1) &= T^{-1}AT\tilde{x}(t) + T^{-1}Bu(t) \\y(t) &= CT\tilde{x}(t) + Du(t)\end{aligned}\tag{Equation 2-7}$$

Therefore, the goal of system identification is to identify the contents of A, B, C and D from the experimental data in a minimal realization of state space form. Here, the subspace system

identification method is chosen to solve this problem, since it can efficiently propose a suitable model without iterations whose order the user can define arbitrarily (Overchee and Moor 1996).

The algorithms are based on the following observations:

1. Supposing that the extended observability matrix in Equation 2-8 for the system are known, then the matrices C and A are obtainable. Extracting C from the first block row of O_r and using the shift properties to solve A :

$$O_r = \begin{bmatrix} C \\ CA \\ \vdots \\ CA^{r-1} \end{bmatrix} \quad \text{Equation 2-8}$$

$$CA^{r-1} = (CA^{r-1})A \quad \text{Equation 2-9}$$

The latter step as shown in Equation 2-9 should be solved in least square sense since inevitable noise is present in the data.

2. If A and C are known, B and D can be estimated using the predictor form presented in Equation 2-10 :

$$y(t|B, D) = C(qI - A)^{-1}Bu(t) + Du(t) \quad \text{Equation 2-10}$$

where q is the time shift operator.

It can be observed that Equation 2-10 is clearly linear in B and D , and therefore B and D can be solved by using least square method.

3. The extended observability matrix can be consistently estimated from the input-output data by direct least-square-like (projection) steps.

The flow chart of the subspace system identification is presented in Figure 2-5 to illustrate the concept. First, the extended observability matrix is obtained by using the input-output data to

form a matrix that is related to O_r , and then the singular value decomposition (SVD) is implemented to find out O_r . It should be noted that, from the SVD, the user can choose model order (matrix size in Equation 2-6) suitable to retain the most significant values of the singular equivalencies to achieve the purpose of the model order reduction. QR decomposition is the numerical tool of choice to implement this step. After the extended observability matrix, O_r , is constructed from the input-output data, C can be directly obtained from O_r , and A can be calculated using Equation 2-9 in the least square sense. After A and C are known, B and D can be calculated using the least square method shown in Equation 2-10. A detailed explanation can be found in Overchee and Moor (1996) and Ljung (1999).

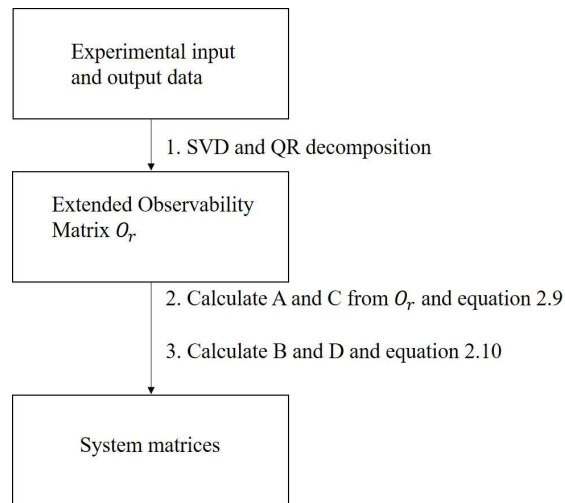


Figure 2-5 Subspace system identification flow chart

The Hokkaido earthquake ground motion is used to conduct the system identification test. The input-output data are plotted in Figure 2-6 and the fitting result is plotted in Figure 2-7. The hydraulic actuator model in state space form is presented in Equation 2-11.

$$\dot{x} = Ax + Bu$$

$$y = Cx + Du$$

$$A = \begin{bmatrix} -0.04231 & -2.193 & -0.1573 \\ 1.876 & -29.21 & 125.1 \\ -1.674 & -100.2 & -26.93 \end{bmatrix}, B = \begin{bmatrix} 1.895 & 0.3166 \\ 22.12 & 5.854 \\ 87.13 & 13.63 \end{bmatrix}$$

$$C = [1881 \quad -3.858 \quad -0.5678], D = [0 \quad 0] \quad \text{Equation 2-11}$$

It should be noted that the state space model can be converted to the transfer function model by using the transformation relationship in Equation 2-12. In other words, the state space model for the hydraulic actuator can be transformed into two transfer functions, since it requires two inputs and one output. This fact perfectly aligns with the model structure described previously. The two transfer functions are presented in Equation 2-13 and Equation 2-14, and these two transfer functions are identical to the two transfer functions, ($G_1(s)$ and $G_2(s)$), presented in Figure 2-2.

$$G(s) = \frac{Y(s)}{U(s)} = C(s * I - A)^{-1} B + D \quad \text{Equation 2-12}$$

$$G_1(s) = \frac{3430s^2 + 3.86 * 10^4 s + 403.3}{s^3 + 56.18s^2 + 1.333 * 10^4 s + 178.2} \quad \text{Equation 2-13}$$

$$G_2(s) = \frac{565.1s^2 - 1818s + 3.12 * 10^5}{s^3 + 56.18s^2 + 1.333 * 10^4 s + 178.2} \quad \text{Equation 2-14}$$

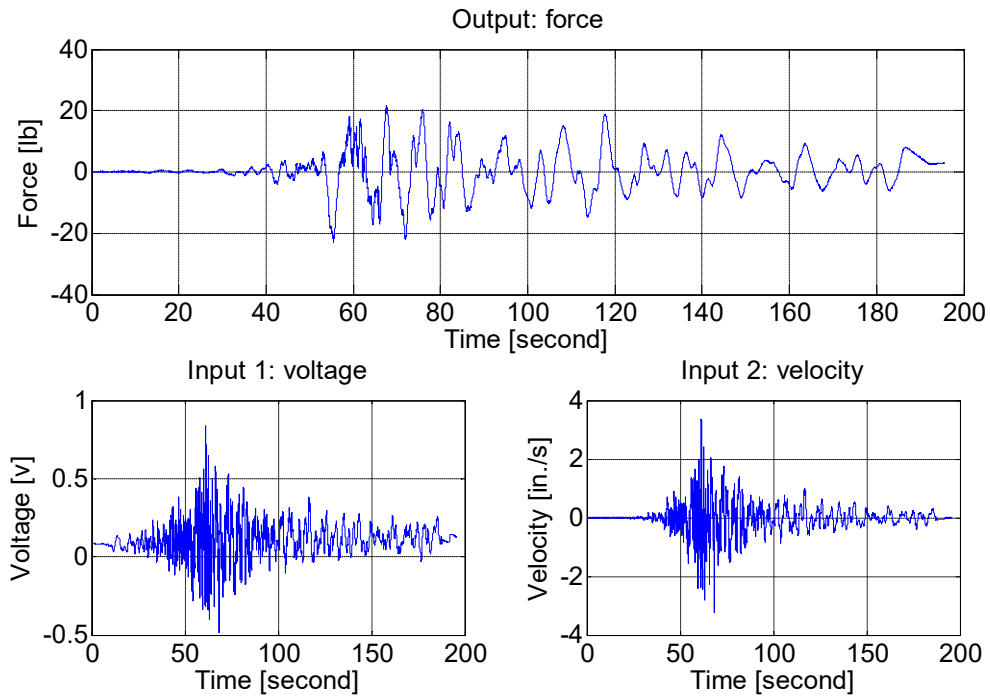


Figure 2-6 Input and output data for hydraulic actuator model

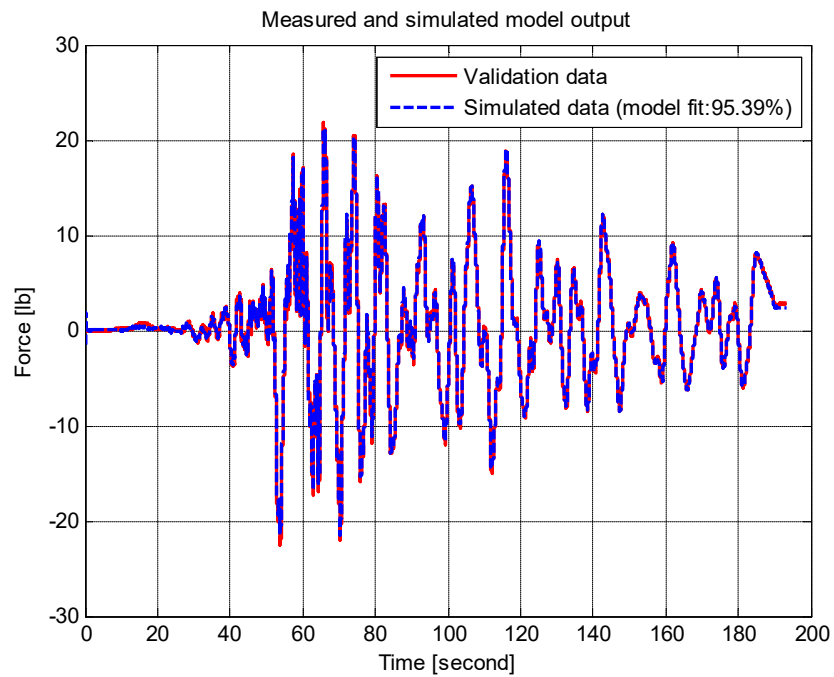


Figure 2-7 Simulation model fit for hydraulic actuator

2.3.3 System Identification for Shake Table

The second order transfer function is used to describe shake table dynamics. Since the numerator and denominator order are known in this case, the identification problem is to ascertain the parameters for Equation 2-5. The method presented in this section utilizes the Gauss-Newton method (Nocedal and Wright 1999) to do the iterative parameter estimation. This method uses the gradient and Hessian matrix to determine the minimum point of the parameter estimation error. However, this method requires a good initial point to begin and, therefore, the instrumental variable (IV) method in conjunction with the state variable filter (SVF) is adopted to provide the initial guess for the Gauss-Newton method (Ljung 2009). The flow chart of the transfer function parameter estimation is shown in Figure 2-8.

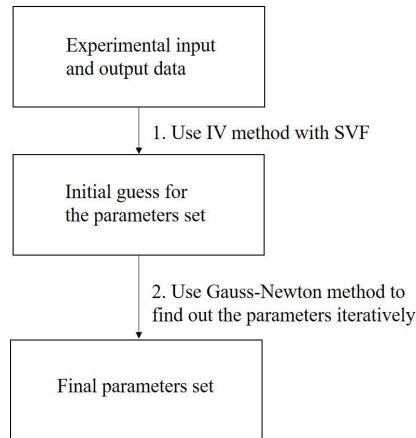


Figure 2-8 Transfer function parameters estimation procedure

Consider the following general transfer function form in Equation 2-15. By performing the inverse Laplace transformation, the input and output relationships can be formulated as Equation 2-16:

$$G(s) = \frac{Y(s)}{U(s)} = \frac{b_1 s^{m-1} + b_2 s^{m-2} \dots + b_m}{s^n + a_1 s^{n-1} + \dots + a_n} \quad \text{Equation 2-15}$$

$$y^{(n)}(t) + a_1 y^{(n-1)}(t) + \dots + a_n y(t) = b_1 u^{(m-1)}(t) + b_2 u^{(m-2)}(t) \dots + b_m u(t) \quad \text{Equation 2-16}$$

where $y^{(k)}(t)$ denotes the kth derivative of $y(t)$ with respect to time and assume $n \geq m$.

It should be noted that $u(t)$ and $y(t)$ are the input and output time history data, respectively. Equation 2-16 can be converted as a linear regression by implementing a continuous time filter $L(s)$ defined in Equation 2-17 to low pass the Equation 2-16. As performed in Equation 2-18 and Equation 2-19, Equation 2-16 can be transformed as a perfect linear regression, as in Equation 2-20. $L(s)$ is called State Variable Filter (SVF).

$$L(s) = \left(\frac{\lambda}{s + \lambda} \right)^n \quad \text{Equation 2-17}$$

$$z_k(t) = L(s)y^{(k)}(t) \quad \text{Equation 2-18}$$

$$\omega_k(t) = L(s)\omega^{(k)}(t) \quad \text{Equation 2-19}$$

$$z_n(t) + a_1 z_{n-1}(t) + \dots + a_n z_0(t) = b_1 \omega_{m-1}(t) + b_2 \omega_{m-1}(t) \dots + b_m \omega_0(t) \quad \text{Equation 2-20}$$

The Equation 2-20 will have well-defined quantities, and can be reformulated, at the sampling instants $t = t_j$, as the standard linear regression form as presented in Equation 2-21.

$$z_n(t|\theta) = \varphi^T(t)\theta + v_0(t)$$

$$\varphi^T(t) = [-z_{n-1}(t) \quad \dots \quad -z_0(t) \quad \omega_{m-1}(t) \quad \dots \quad \omega_0(t)]$$

$$\theta = [a_1 \quad \dots \quad a_n \quad b_1 \quad \dots \quad b_m] \quad \text{Equation 2-21}$$

where $v_0(t)$ is defined as the generalized equation error from the measurement noise.

The general solution to Equation 2-21 is to use the least square method. However, the results of the least square method will be biased due to the existence of the measurement noise. Hence, the instrumental variable (IV) method is used to solve this linear regression problem and

provide an initial value for the parameters (Garnier *et al.* 2003). The IV estimate for the parameters is given in Equation 2-22. The detailed explanation can be found in Section 7.6 in Ljung (1999).

$$\hat{\theta} = \left(\sum_j \zeta(t_j) \varphi^T(t_j) \right)^{-1} \sum_j \zeta(t_j) z_n(t_j) \quad \text{Equation 2-22}$$

where $\zeta(t_j)$ is the instrument vector and t_j is the sampling instant.

Once the initial value of the parameter set is obtained, the Gauss-Newton method (Wright and Nocedal 1999) can be applied to iteratively optimize the fitting error. The optimization problem can be formulated as the nonlinear least square problem, as shown in Equation 2-23:

$$f(\theta) = \frac{1}{2} \sum_{j=1}^m r_j^2(\theta) = \frac{1}{2} \sum_{j=1}^m (z_n(j) - \varphi^T(j)\theta)^2 \quad \text{Equation 2-23}$$

The Gauss-Newton method is a line search method facilitating discovery of the best θ to achieve the minimum value for Equation 2-23. The standard form for the line search method is shown in Equation 2-24:

$$\theta_{k+1} = \theta_k + \alpha_k p_k \quad \text{Equation 2-24}$$

where k is the iteration, α_k is the step length and p_k is the search direction.

In the Gauss-Newton method, the step length, α_k , is selected as 1 and the search direction is defined using the following procedure. First, the residual vector $r(\theta)$ is defined from Equation 2-24. The Jacobian matrix can be found in Equation 2-26. It should be noted that n is the dimension of θ . Next, the search direction can be found in Equation 2-27

$$r(\theta) = (r_1(\theta), r_2(\theta), \dots, r_m(\theta))^T \quad \text{Equation 2-25}$$

$$J(\theta) = \left[\frac{\partial r_j}{\partial \theta_i} \right]_{j=1 \dots m, i=1 \dots n} \quad \text{Equation 2-26}$$

$$p_k = (J_k^T J_k)^{-1} (-J_k^T) r_k \quad \text{Equation 2-27}$$

The transfer function of the shake table with an equivalent mass is obtained and presented in Equation 2-28, which is identical to the $G_{table}(s)$ presented in Figure 2-2. The input-output data and the fitting result are plotted in Figure 2-9 and Figure 2-10.

$$G_{table}(s) = \frac{8.248}{s^2 + 2.034s + 192.4} \quad \text{Equation 2-28}$$

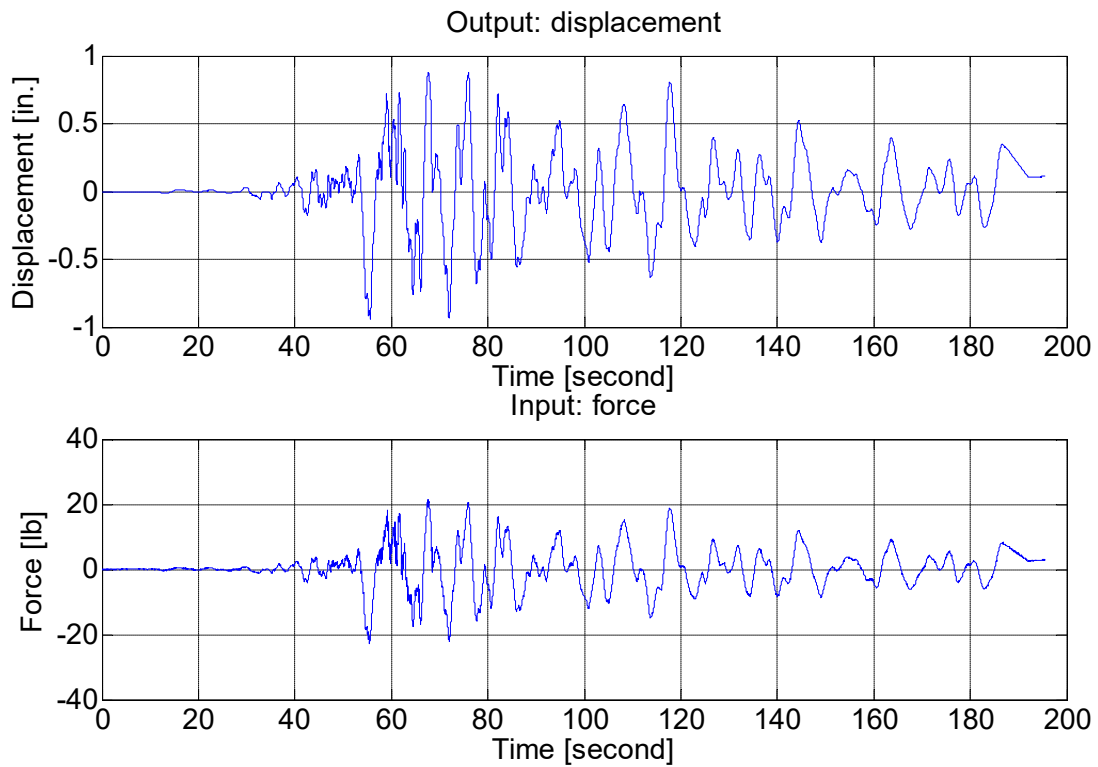


Figure 2-9 Input and output data for shake table model

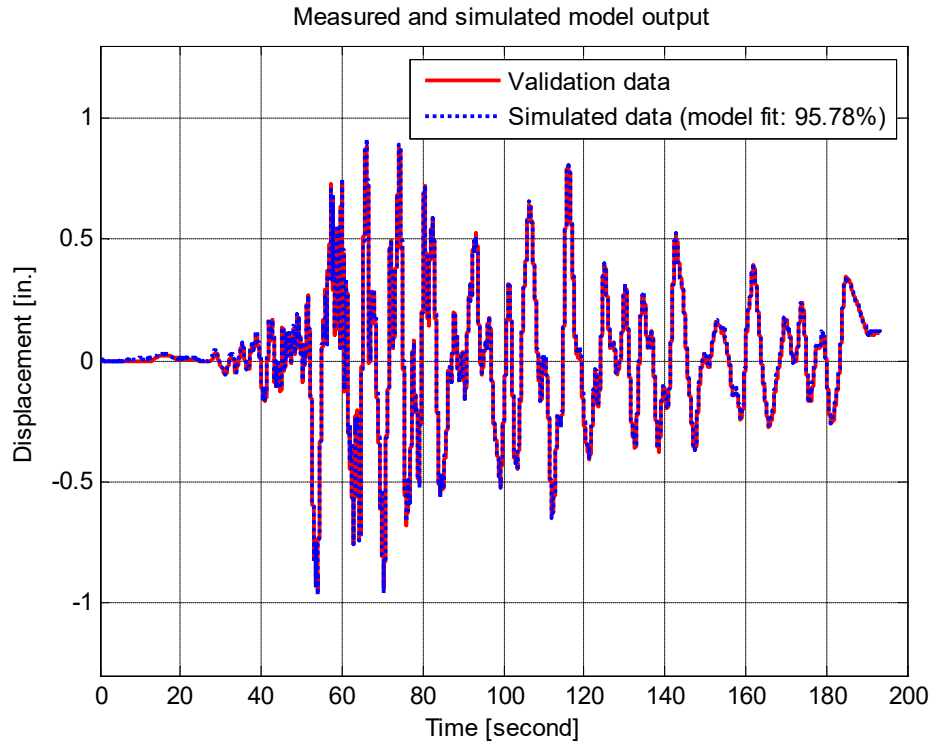


Figure 2-10 Measured and simulated model output for shake table model

2.4 Summary

In this chapter, the system identification concept and procedure are introduced to construct the precise simulation model for control design purposes. The hydraulic actuator dynamics are investigated through physical equation derivation. From the results of the physical equations, it can be observed that the hydraulic actuator force is generated by the voltage input and actuator velocity feedback. Since the hydraulic actuator is attached to the shake table, the velocity of the actuator is equal to the velocity output of the shake table. This essentially demonstrates that the shake table and specimen dynamics will influence the hydraulic actuator dynamics; this phenomenon is termed the CSI effect. Therefore, the shake table and specimen dynamics should be considered for the controller design and tuning phase.

To obtain the precise simulation model for the hydraulic shake table system, the grey box modeling method is chosen. A scaled one degree of freedom hydraulic shake table platform is constructed in the structure lab at UBC. The experimental data are collected using the real-time control system provided by ACTS. The subspace system identification method is employed to fit the numerical state-space model obtained from the experimental data. The model for the hydraulic actuator and the shake table with its specimen are constructed separately. The fitting result shows the high fidelity of the proposed system identification method, and the controller design in the following chapters will utilize the model assembled in Chapter 2.

Chapter 3: Low-level Controller Design

3.1 Overview

The dynamics for the hydraulic shake table system is investigated and the simulation model generated from the experimental data found in Chapter 2. To implement the hierarchical control strategy, a low-level controller is required to control the hydraulic actuator. In this chapter, the low-level controller design technique is introduced to design a controller to stabilize the hydraulic shake table and achieve basic tracking performance. The control techniques in this chapter include the proportional-integral-differential (PID), three-variable- (TVC) and loop-shaping control. The frequency response and experimental data are presented to prove that the model-based controller design can replace the traditional blind tuning method, while saving the time and expenditure required in the real laboratory.

3.2 PID Control

3.2.1 Theory

The PID control is the most popular and successfully applied technique in the control engineering field. Due to its simplicity and convenience, it has been considered a good solution for industrial applications. The block diagram for PID control is presented in Figure 3-1, where r is the reference input, e is the error term, u is the control signal and y is the measured output. The error term is the difference between the reference signal and the measured output.

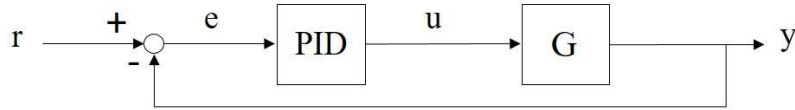


Figure 3-1 PID control block diagram

The PID controller utilizes a proportional, integral and derivative calculation to generate the control input signal, which is aimed to minimize the error term and achieve the tracking purpose. A typical PID controller can be formulated as the following expression:

$$u(t) = k_p e + k_I \int_0^t e dt + k_D \frac{de}{dt} \quad \text{Equation 3-1}$$

where k_p , k_I , k_D are the proportional, integral, derivative gain, respectively.

To decrease rise time, which means increasing the system response speed and bandwidth, the proportional gain can be raised, but this will decrease the system stability margin and reduce control robustness. The integral gain will eliminate steady state error and improve system accuracy. The non-zero value for the error term will be integrated over time until it is sufficiently large to move the plant output state to its final position. The derivative gain is used to decrease the overshoot problem, which improves the system's stability at a higher proportional gain. In the hydraulic actuator control application, the P controller is usually implemented first to achieve basic close-loop control. Null shifts always occur on servo valve dynamics, so the integral action will appear to improve the tracking accuracy. The effects of the three gains in PID controller are listed in Table 3-1.

Table 3-1 PID control gain effect

Close Loop Response	Rise Time	Overshoot	Settling Time	Steady-state error
k_p	Decrease	Increase	Small Change	Decrease

Table 3-1 PID control gain effect

k_I	Decrease	Increase	Increase	Eliminate
k_D	Small Change	Decrease	Decrease	No change

3.2.2 PID Controller Design

In the traditional tuning procedure, the user needs to tune the gain based on the rules on site by trial and error illustrated in Table 3.1. Classical tuning methods include that of Ziegler-Nichols. However, this method is time-consuming and inefficient, while lacking the mathematical proof to state its system stability and performance.

Therefore, in this chapter, the model constructed in Chapter 2 is utilized to provide a mathematical tuning solution. The block diagram for integrating the PID controller with the hydraulic shake table system is shown in Figure 3-2. From this figure, the velocity of the shake table can be presented, as shown in Equation 3-2.

$$\dot{x} = G_3 s F \tag{Equation 3-2}$$

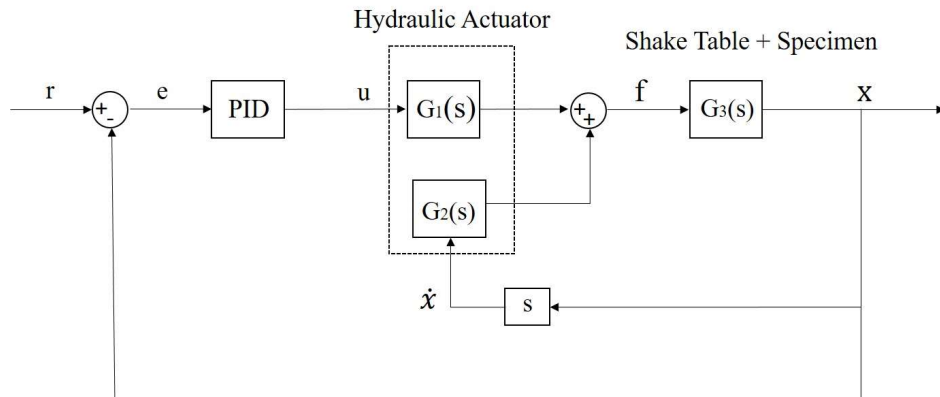


Figure 3-2 PID control in hydraulic shake table system

Combining Equation 2-4 and Equation 3-2, the transfer functions for voltage to displacement and voltage to force can be calculated; the process is presented in Equation 3-3, Equation 3-4 and Equation 3-5:

$$G_1u + G_2G_3sF = F \quad \text{Equation 3-3}$$

$$G_{uF} = \frac{F}{u} = \frac{G_1}{1 - G_2G_3s} \quad \text{Equation 3-4}$$

$$G_{ux} = \frac{x}{u} = \frac{G_1G_3}{1 - G_2G_3s} \quad \text{Equation 3-5}$$

where G_{uF} is the voltage to force transfer function and G_{ux} is the voltage to displacement transfer function.

Since the high-level controller presented in Chapter 4 requires both the displacement and force controllers to be in the low-level control phase, the designs for both of these controllers are presented in this section. The frequency response plots for the displacement and force controller designs are presented in Figure 3-3 and Figure 3-4. The displacement and force controllers are listed in Equation 3-6 and Equation 3-7.

$$C_d = \frac{3s + 0.4}{s} \quad \text{Equation 3-6}$$

$$C_f = \frac{0.366s + 3.222}{s} \quad \text{Equation 3-7}$$

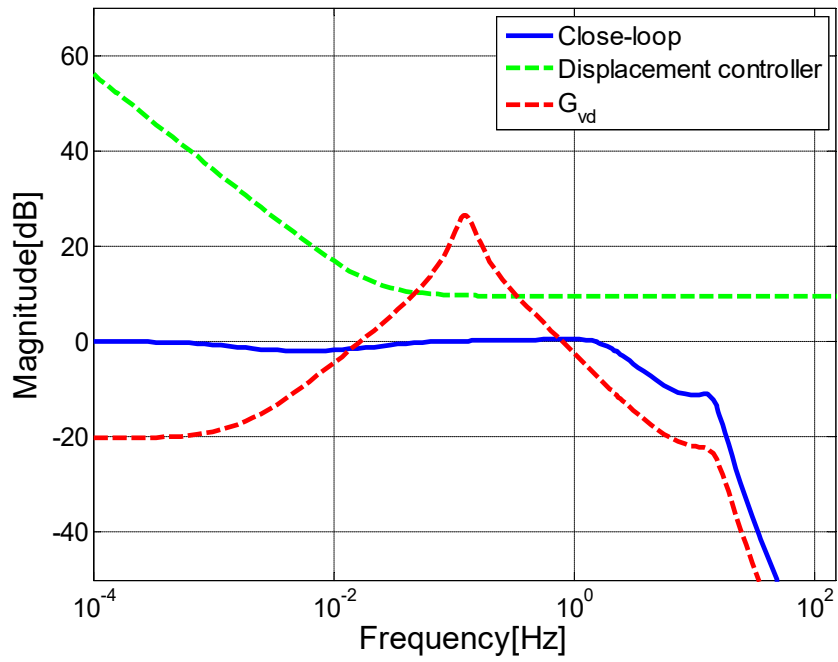


Figure 3-3 Displacement PID controller design

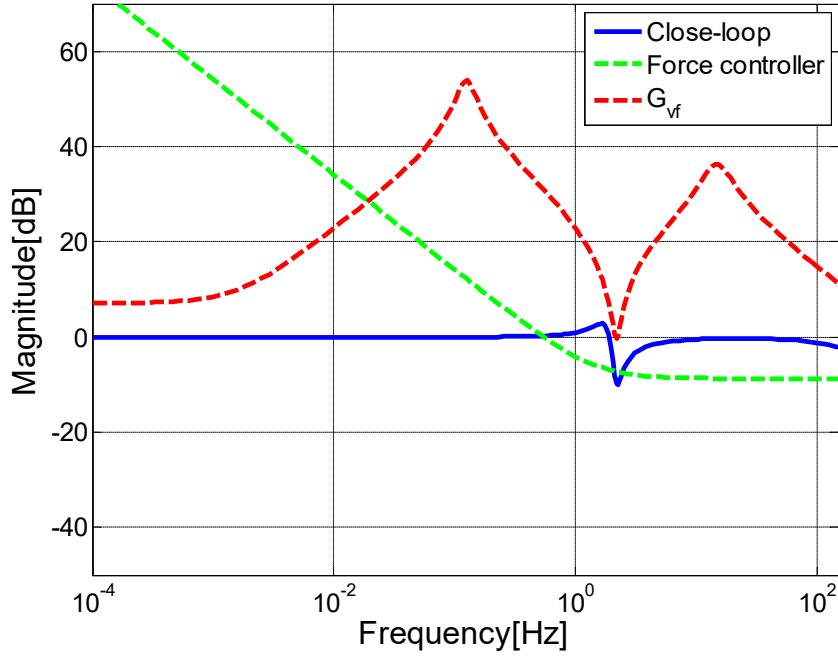


Figure 3-4 Force PID controller design

3.3 Three Variable Control

The displacement based control method using the PID controller introduced in Section 3.2 is widely implemented on various shake tables worldwide. Nevertheless, the standard requirement for the shake table test is the high frequency tracking conducted in the acceleration trajectory, for which PID control is unable to achieve sufficient bandwidth. Therefore, the velocity and acceleration control loops are employed to increase the control bandwidth; this control technique is labelled three-variable-control (TVC). The full control structure for TVC is illustrated in Figure 3-5. r, \dot{r} and \ddot{r} are the reference displacement, velocity and acceleration and x, \dot{x} and \ddot{x} are the measured displacement, velocity and acceleration of the shake table, respectively. TVC can be divided into two parts, those of feedback and feedforward control. The feedback control portion's main issue is to guarantee control stability, while feedforward control aims to increase tracking performance. It should be noted that, in this chapter, the PID controller is used to replace displacement feedback gain to improve performance.

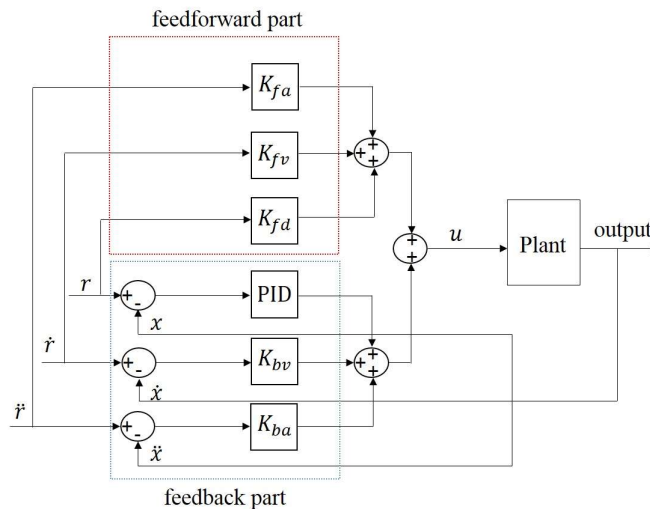


Figure 3-5 Control structure for proposed TVC

The simulation framework is built in the Simulink environment and the model introduced in Chapter 2 is used to simulate plant dynamics. The gain setup for the TVC is presented in Table 3-2. The time and frequency domains' tracking responses for the 1980 Irpinia Italy earthquake record obtained from PEER are presented in Figure 3-6 and Figure 3-7. From both time and frequency domain observations, it can be clearly seen that the TVC can outperform the PID in acceleration trajectory tracking. In Chapter 5, the TVC is utilized as a low-level controller.

Table 3-2 Gain setup for TVC

Gain	P	I	D	K_{bv}	K_{ba}	K_{fd}	K_{fv}	K_{fa}
Value	6.15	0.161	0	0.005	0.0001	0.2	0.125	0

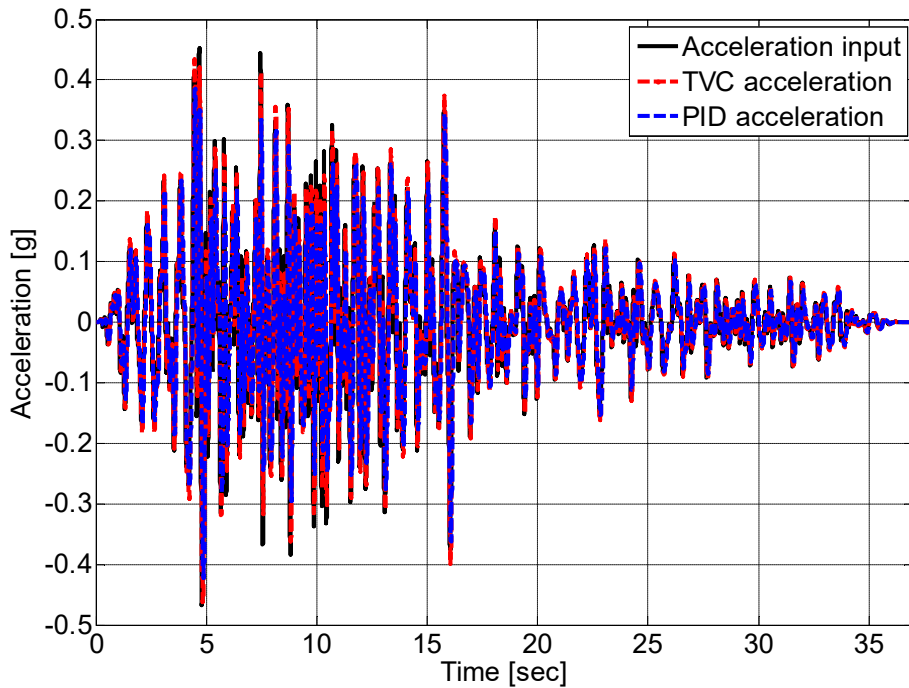


Figure 3-6 Time domain comparison for TVC and PID control

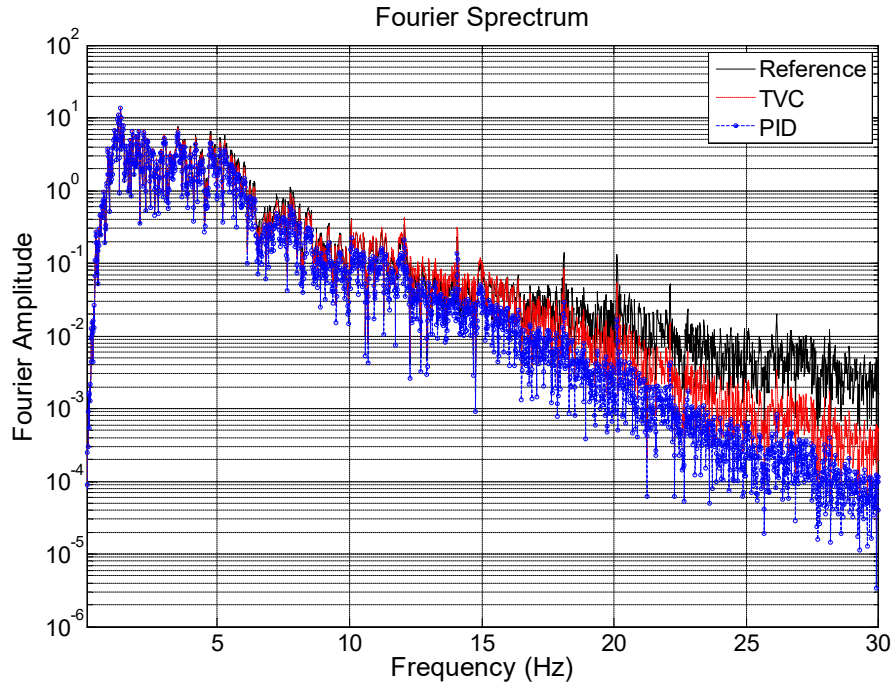


Figure 3-7 Frequency domain comparison for TVC and PID control

3.4 Loop-shaping Control

Loop-shaping control is another commonly used linear control design technique. It utilizes the frequency response from the plant model and generates a controller to shape the open-loop frequency response to the desired shape and meet the design specifications. Figure 3-8 is the loop-shaping control block diagram.

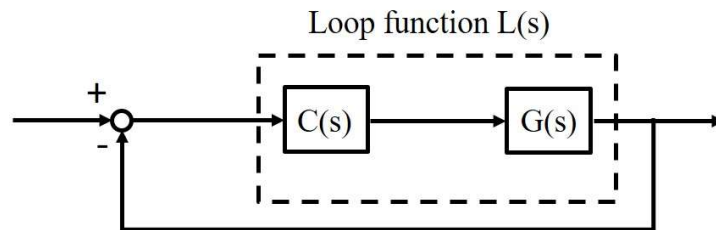


Figure 3-8 Loop-shaping control block diagram

Loop-shaping control mainly consists of designing the frequency domain response of the loop function $L(s)$ to satisfy control system requirements such as bandwidth, and gain and phase

margins. In this section, the loop function $L(s)$ is designed as presented in Equation 3-8, with ω_n representing the desired crossover frequency. With the loop function design in Equation 3-8, the close-loop transfer function can be calculated in Equation 3-9, which has the desired frequency response. From the transfer function of the plant $G(s)$ obtained from Equation 3-5, the controller transfer function $C(s)$ can be calculated using H-infinity synthesis (McFarlane and Glover 1992), so that the desirable loop function $L(s)$ is realized. By changing the value of ω_n , the bandwidth of the overall system can be adjusted and, therefore, higher quality frequency domain tracking can be achieved. The second order loop-shaping controller is presented in Equation 3-10:

$$L(s) = C(s)G(s) = \frac{\omega_n}{s} \quad \text{Equation 3-8}$$

$$T(s) = \frac{L}{1+L} = \frac{\omega_n}{s + \omega_n} \quad \text{Equation 3-9}$$

$$C_{LS} = \frac{6.986(s^2 + 0.2975s + 0.5892)}{s(s + 0.01046)} \quad \text{Equation 3-10}$$

Figure 3-9 presents the frequency response plot for the loop-shaping controller design. A comparison between the close-loop response of using the loop-shaping and PID controllers is presented in Figure 3-10; from this, it can be observed that the loop-shaping controller can achieve a better frequency response. It can thus be concluded that the loop-shaping controller design fully utilizes the information from the simulation model that obtained from Chapter 2, achieving better performance than the traditional PID controller. The loop-shaping controller is chosen as the benchmark controller in Chapter 4.

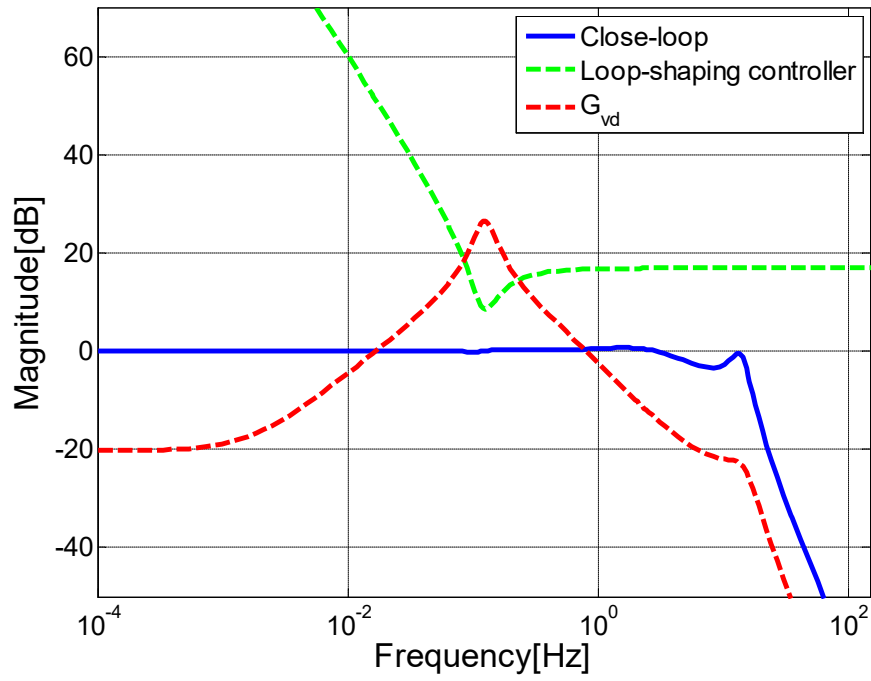


Figure 3-9 Loop-shaping controller design

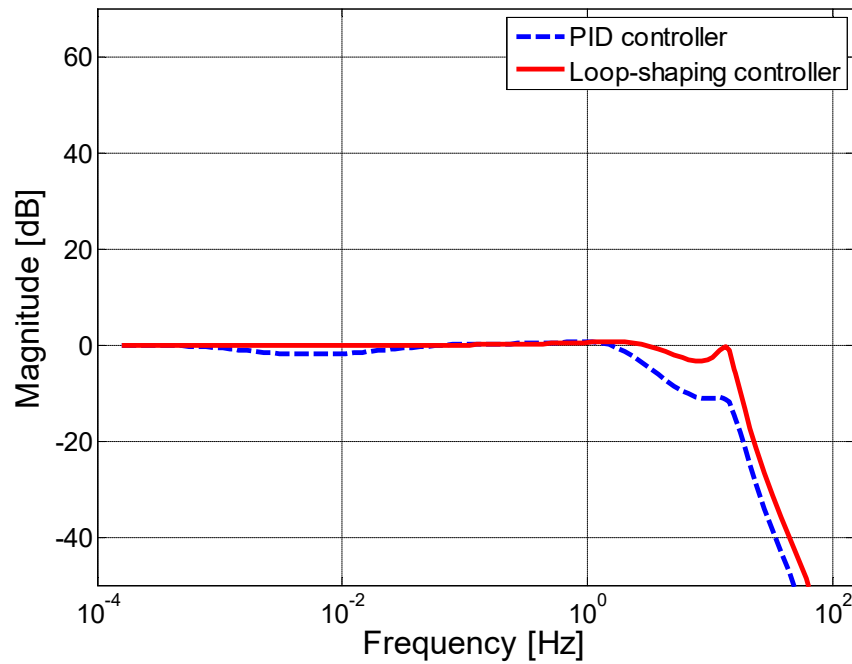


Figure 3-10 Close-loop response comparison between PID and loop-shaping controller

3.5 Summary

Three low-level controller design methods are presented in this chapter. The PID control theory and the gain effect are introduced. The traditional method for tuning simply involved the user's tuning the gain based on trial and error. The model-based design procedure which utilizes the model obtained from Chapter 2 is presented as a substitute for traditional tuning. The model-based method can reduce costs, while performing feasible stability analysis. The TVC method is also presented in this chapter, with its advantage being that it achieves a higher bandwidth than the PID control, as is proven here through simulation result analyses in both the time and frequency domains. Finally, the loop-shaping control method is introduced as a frequency domain design method. It utilizes the frequency response of the plant model, and compensates it to the desired shape while achieving the design specifications. These controllers will be used in the following chapters to support the high-level controller design.

Chapter 4: Sliding Mode Control

4.1 Theory Background

Sliding mode control (SMC) originates from the Lyapunov theory, a commonly used theorem for conducting nonlinear stability analyses and controller designs. Two methods have been introduced in Lyapunov theory: the linearization and direct methods. The linearization method draws its conclusions about a nonlinear system's local stability around an equilibrium point from the stability properties of its linear approximated model. In other words, the linearization method claims that the stability properties of a nonlinear system in the close area of an equilibrium point are essentially identical to those of its linearized approximation. This method provides the theoretical justification for implementing linear control in a nonlinear system. However, this approach shows that linear controller implementation is a matter of consistency; namely, that the controller design must have the ability to restrict the system within its linear range. However, it is often difficult to precisely define the linear range, motivating the development of the direct method.

The direct method is not restricted to local motion near the equilibrium point. It determines the stability properties from the viewpoint of the system's total energy. The basic concept of the direct method arises from a fundamental physical observation that, if the total energy of a mechanical system is continuously dissipated, regardless of whether the system is linear or nonlinear, the system must eventually arrive at an equilibrium point. Considering the nonlinear

mass-spring-damper system in Figure 4-1 as an example, the equation of motion for the mechanical system can be listed in Equation 4-1.

$$m\ddot{x} + b\dot{x}|\dot{x}| + k_0x + k_1x^3 = 0 \quad \text{Equation 4-1}$$

where $b\dot{x}|\dot{x}|$ is the nonlinear damping term and $k_0x + k_1x^3$ is the nonlinear spring term.

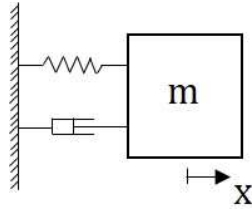


Figure 4-1 Lyapunov theory example: nonlinear mass spring damper system

It would be difficult to conduct a stability analysis for this system using the definitions of stability, since the general solution to this nonlinear equation is unavailable, but the alternative method using the system's energy provides a feasible solution for this kind of nonlinear system. The total mechanical energy of this system is the sum of its kinetic and its potential energy, which can be written in Equation 4-2:

$$\begin{aligned} V(x) &= \frac{1}{2}m\dot{x}^2 + \int_0^x (k_0x + k_1x^3)dx \\ &= \frac{1}{2}m\dot{x}^2 + \frac{1}{2}k_0x^2 + \frac{1}{4}k_1x^4 \end{aligned} \quad \text{Equation 4-2}$$

By taking the derivative of Equation 4-2 and combining it with Equation 4-1, Equation 4-3 can be derived, which shows the changing rate of the above system:

$$\dot{V}(x) = m\dot{x}\ddot{x} + (k_0x + k_1x^3)\dot{x} = \dot{x}(-b\dot{x}|\dot{x}|) = -b|\dot{x}|^3 \quad \text{Equation 4-3}$$

The relationships between mechanical energy and stability can be observed from the above derivation and concluded in the following three points:

1. Zero energy corresponds to the equilibrium point ($x = 0, \dot{x} = 0$)
2. Asymptotic stability means the convergence of mechanical energy to zero
3. Instability is related to the growth of mechanical energy

Equations 4.2 and Equation 4-3 imply the fact that the total mechanical energy of the above system begins from an initial value and is continuously dissipated by the damper until the mass halts its motion ($\dot{x} = 0$), and that, even without an analytical solution, the system's stability can be guaranteed. Lyapunov's direct method is based on the generalization of this concept in the above case to more complex systems. The procedure of Lyapunov's direct method is to generate a scalar "energy-like" function (i.e. positive definite) for the dynamic system, and examine the time variation of that scalar function. If the scalar function is decreasing, which means the derivative of the scalar function is negative definite, then the dynamic system is guaranteed to be globally stable. It should be noted that the Lyapunov theory can also be applied to controller designs, with one famous example being the sliding mode control (SMC) illustrated in this chapter.

SMC is a nonlinear control technique featuring remarkable properties of accuracy, robustness, easy tuning and implementation (Utkin 1977). SMC systems are designed to drive the system states onto a designed surface in the state space termed the sliding surface. Once the sliding surface is reached, sliding mode control retains the states close to the sliding surface. Hence, the sliding mode control can be separated into two parts. The first involves the sliding surface design, such that the sliding motion satisfies the design specifications. The second is concerned with choosing a control law that will make the switching surface attractive to the system state. In the control law selection phase, the Lyapunov theory is used to guarantee stability and convergence (Slotine 1991).

There are two main advantages to sliding mode control. The first is that the dynamic behavior of a system may be tailored by the choice of the sliding function. Secondly, the closed loop response can become totally insensitive to uncertainties. From a practical point of view, the SMC allows for controlling nonlinear processes subject to external disturbances and heavy model uncertainties. This advantage makes SMC a preferable choice than other alternative linear control approaches for shake table control. Moreover, rapid asymptotical convergence can also be obtained with the SMC.

4.2 Control Law Derivation

Figure 4-2 shows a simplified unidirectional shake table model with a single degree of freedom (SDOF) specimen. The equations for the motion of the specimen and shake table are defined in Equation 4-4 and Equation 4-5. As will be explained later, the high-level controller will calculate force command signals based on the system's dynamics. The low-level controller(s) will regulate the table based on the command signals.

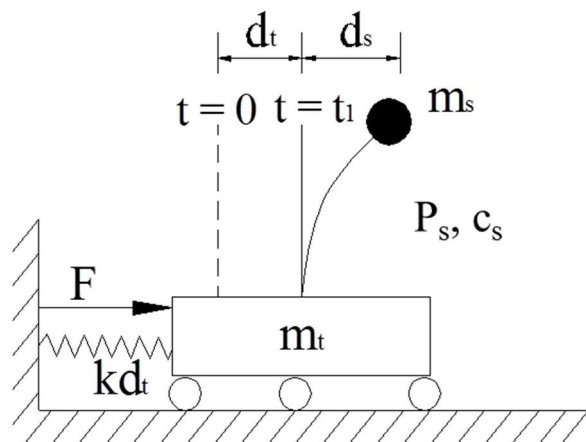


Figure 4-2 Schematic plot of the SDOF shake table model

$$m_s(\ddot{d}_t + \ddot{d}_s) + c_s \dot{d}_s + P_s(d_s, \dot{d}_s) = 0 \quad \text{Equation 4-4}$$

$$m_t \ddot{d}_t - c_s \dot{d}_s - P_s(d_s, \dot{d}_s) - F + kd_t = 0 \quad \text{Equation 4-5}$$

The setup has a table mass of m_t and a specimen lump mass of m_s . Two measured displacements are defined. d_t represents the relative displacement of the table with respect to the ground, while d_s represents the relative displacement at the top of the specimen with respect to the table. c_s is the damping constant of the specimen, and \dot{d}_s is the relative velocity of the specimen. \ddot{d}_t represents the acceleration of the table, while \ddot{d}_s denote the relative acceleration of the specimen. F represents the applied force to the system. To obtain force feedback, the table is connected to a reaction wall with linear springs whose stiffness is denoted as k . The resulting spring force experienced by the table is kd_t . The specimen resisting force, P_s , is typically nonlinear and will influence the control performance.

Equation 4-4 and Equation 4-5 can be transformed into a state space representation as described by Equation 4-6.

$$\begin{Bmatrix} x_1 \\ x_2 \\ x_3 \\ x_4 \end{Bmatrix} = \begin{Bmatrix} d_t \\ \dot{d}_t \\ d_s \\ \dot{d}_s \end{Bmatrix}$$

$$\begin{Bmatrix} \dot{x}_1 \\ \dot{x}_2 \\ \dot{x}_3 \\ \dot{x}_4 \end{Bmatrix} = \begin{Bmatrix} x_2 \\ \frac{1}{m_t} (P_s(x_3, x_4) + c_s x_4 + F - kx_1) \\ x_4 \\ -\frac{1}{m_t} (P(x_3, x_4)_s + c_s x_4 + F - kx_1) - \frac{1}{m_s} (P_s(x_3, x_4) + c_s x_4) \end{Bmatrix}$$

Equation 4-6

The SMC algorithm design should begin with the selection of a sliding surface in which the system exhibits its desired behavior. Next, a feedback control law should be determined such that the trajectory of the system in state space can intersect and be confined to the sliding surface. The sliding surface, S , shown in Equation 4-7, is defined as a linear combination of the displacement tracking error, in Equation 4-8, and the velocity tracking error, in Equation 4-9.

$$S = \dot{\tilde{x}}_1 + \lambda \tilde{x}_1 \quad \text{Equation 4-7}$$

$$\tilde{x}_1 \triangleq x_1 - x_{1d} \quad \text{Equation 4-8}$$

$$\dot{\tilde{x}}_1 \triangleq \dot{x}_1 - \dot{x}_{1d} \quad \text{Equation 4-9}$$

where \tilde{x}_1 and $\dot{\tilde{x}}_1$ denote displacement and velocity tracking errors, respectively, x_1 and x_{1d} are the actual and desired displacements, respectively, \dot{x}_1 and \dot{x}_{1d} represent the actual and desired velocities, respectively, and λ is a tuning parameter that is a strictly positive constant.

To prove the existence of a sliding mode, it is normally necessary to resort to the Lyapunov stability theorem introduced in Chapter 4.1. Consider a Lyapunov functional candidate, as shown in Equation 4-10. Taking the derivative of the Lyapunov functional candidate in Equation 4-10 gives Equation 4-11:

$$V(S(x)) = \frac{1}{2} S(x)^2 \quad \text{Equation 4-10}$$

$$\dot{V}(S(x)) = S(x)\dot{S}(x) \quad \text{Equation 4-11}$$

By selecting \dot{S} as Equation 4-12, Equation 4-11 will be negative definite as shown in Equation 4-13. Because V is positive definite and \dot{V} is negative definite, the Lyapunov stability theorem guarantees that $S(x)$ will approach 0 asymptotically. K is the tuning parameter that controls the convergence rate.

$$\dot{S} = -KS \quad \text{Equation 4-12}$$

$$\dot{V} = -KS^2 \quad \text{Equation 4-13}$$

Equation 4-14 can be derived by taking the derivative of Equation 4-7. It should be noted that, since the resisting force of the specimen cannot be measured directly in the real experimental environment, then, by rearranging the form of Equation 4-4, Equation 4-15 can be obtained. The acceleration of the shake table and specimen can be measured directly by the accelerometers. By substituting Equation 4-15 into Equation 4-14, Equation 4-16 can be found. By equating Equation 4-12 and Equation 4-16, the sliding mode control law can be derived, as shown in Equation 4-17:

$$\dot{S} = \ddot{\tilde{x}}_1 + \lambda \dot{\tilde{x}}_1 = \frac{1}{m_t} (P_s + c_s x_4 + F - kx_1) - \ddot{x}_{1d} + \lambda(x_2 - \dot{x}_{1d}) \quad \text{Equation 4-14}$$

$$P_s + c_s \dot{d}_s = -m_s (\ddot{d}_t + \ddot{d}_s) \quad \text{Equation 4-15}$$

$$\dot{S} = CE(\tilde{x}) + \bar{f} + bF \quad \text{Equation 4-16}$$

where $CE(\tilde{x}) = \lambda(x_2 - \dot{x}_{1d})$, $\bar{f} = \frac{1}{m_t} (-m_s(\ddot{x}_2 + \ddot{x}_4) - kx_1) - \ddot{x}_{1d}$, and $b = \frac{1}{m_t}$

$$\begin{aligned}
u \triangleq F &= \frac{-1}{b}(CE(\tilde{x}) + \bar{f} + KS) && \text{Equation 4-17} \\
&= \frac{-1}{b}(CE(\tilde{x}) + \bar{f} + K(\dot{x}_1 - \dot{x}_{1d}) + K\lambda(x_1 - x_{1d}))
\end{aligned}$$

4.3 Implementation

Equation 4-17 can be rearranged as Equation 4-18,

$$F = F_{disp} + F_{v/a} \quad \text{Equation 4-18}$$

where $F_{disp} = m_t \lambda K(x_{1d} - x_1) + kx_1$ and $F_{v/a} = m_t(K + \lambda)(\dot{x}_{1d} - \dot{x}_1) + m_t \ddot{x}_{1d} + m_s(\dot{x}_2 + \dot{x}_4)$

As shown in Equation 4-18, F_{disp} depends only on x_1 , which is d_t , while $F_{v/a}$ depends on \dot{x}_1 , \dot{x}_2 , and \dot{x}_4 which are \dot{d}_t , \ddot{d}_t , and \ddot{d}_s , respectively. The force command due to velocity, inertia of the mass, damping force, and specimen resistance force ($F_{v/a}$) will be implemented through a force-based controller. On the other hand, the force command conducted solely due to displacement (F_{disp}) will be implemented through a displacement-based controller. The displacement command is calculated by dividing F_{disp} by the table spring constant, k . It is noted that, since the force feedback include both forces $F_{v/a}$ and F_{disp} , the total force command for the force-based controllers will be $F_{v/a} + F_{disp}$, as shown. Such an implementation strategy has significant benefit. Generally speaking, the satisfactory acceleration tracking performance would require an actuator with a high bandwidth to respond rapidly to the input signal variation. From fundamental physics and mathematics, force is equal to mass times acceleration, while

displacement is the double integral of acceleration, which means that the displacement control will theoretically possess a lower bandwidth. Therefore, the force controller should be adopted. However, it is well known that stability issues make it difficult to rely solely on a force controller to regulate the movement of the hydraulic actuator, and a certain kind of stabilization mechanism is required. Here, the stabilization mechanism is provided by the displacement-based controller.

Figure 4-3 demonstrates the implementation of the low-level controllers in a series of high-level controllers. The displacement and force controller are obtained from Equation 3-6 and Equation 3-7. It should be noted that the weighing factors of α and β are implemented to allow the user to select the contribution of each of the low-level controllers. In this research, α and β are both chosen as 0.5.

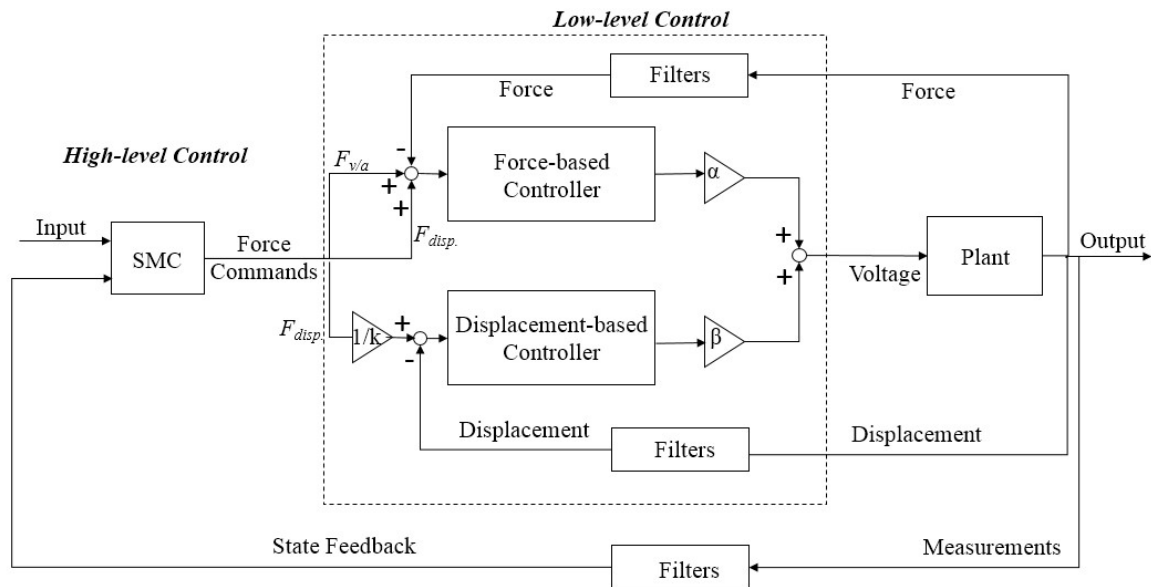
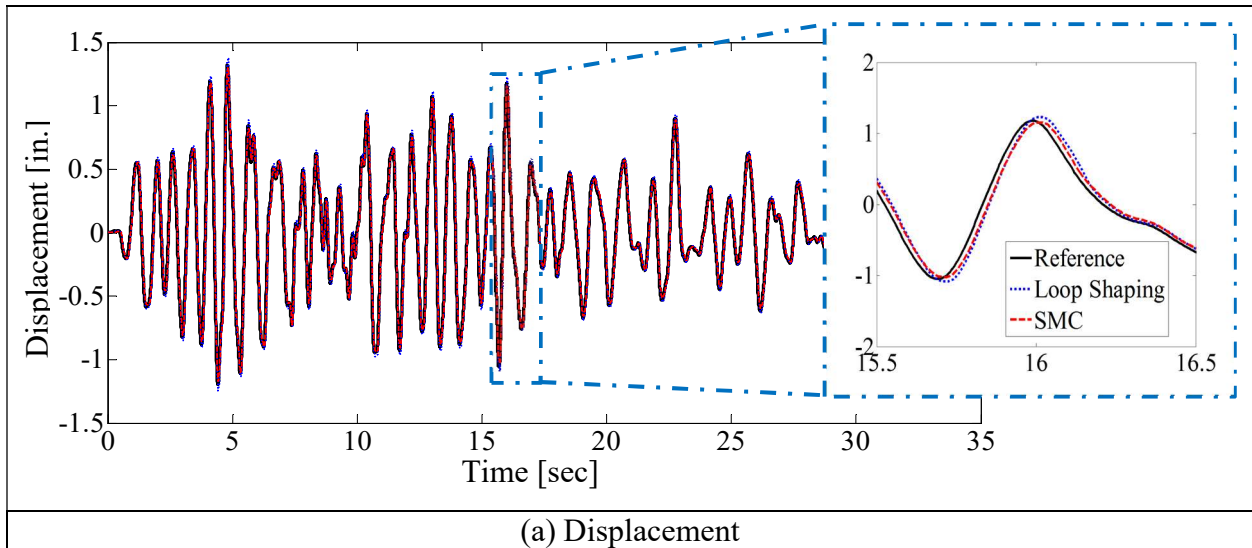


Figure 4-3 Implementation of the hierarchical control architecture of the shake table test

4.4 Experiment Result

The performance of the proposed hierarchical controller is verified with earthquake time-history records. The benchmark controller is designed by using the loop-shaping control technique

illustrated in section 3.4. Figure 4-4 shows the experimental results obtained using the 1980 Irpinia Italy earthquake record as the reference signal. The proposed controller denoted as SMC is compared with the loop shaping displacement-based controller developed in chapter 3. Although both the loop shaping and SMC controllers are able to track the reference displacement well as shown in Figure 4-4 (a), SMC has better tracking capability in velocity and acceleration as shown in Figure 4-4 (b) and Figure 4-4(c), respectively. Figure 4-4 (d) shows the Fourier amplitude plot of the table acceleration. Both controllers perform well at frequencies lower than 7Hz. SMC has better performance in mid to high frequency ranges. Figure 4-5 shows a photo of the damaged yielding plates after the test. Evidently, the system has high nonlinearity and forms plastic hinges at the top and bottom of the plates. The significant nonlinear behavior can also be observed from the specimen hysteresis as shown in Figure 4-6.



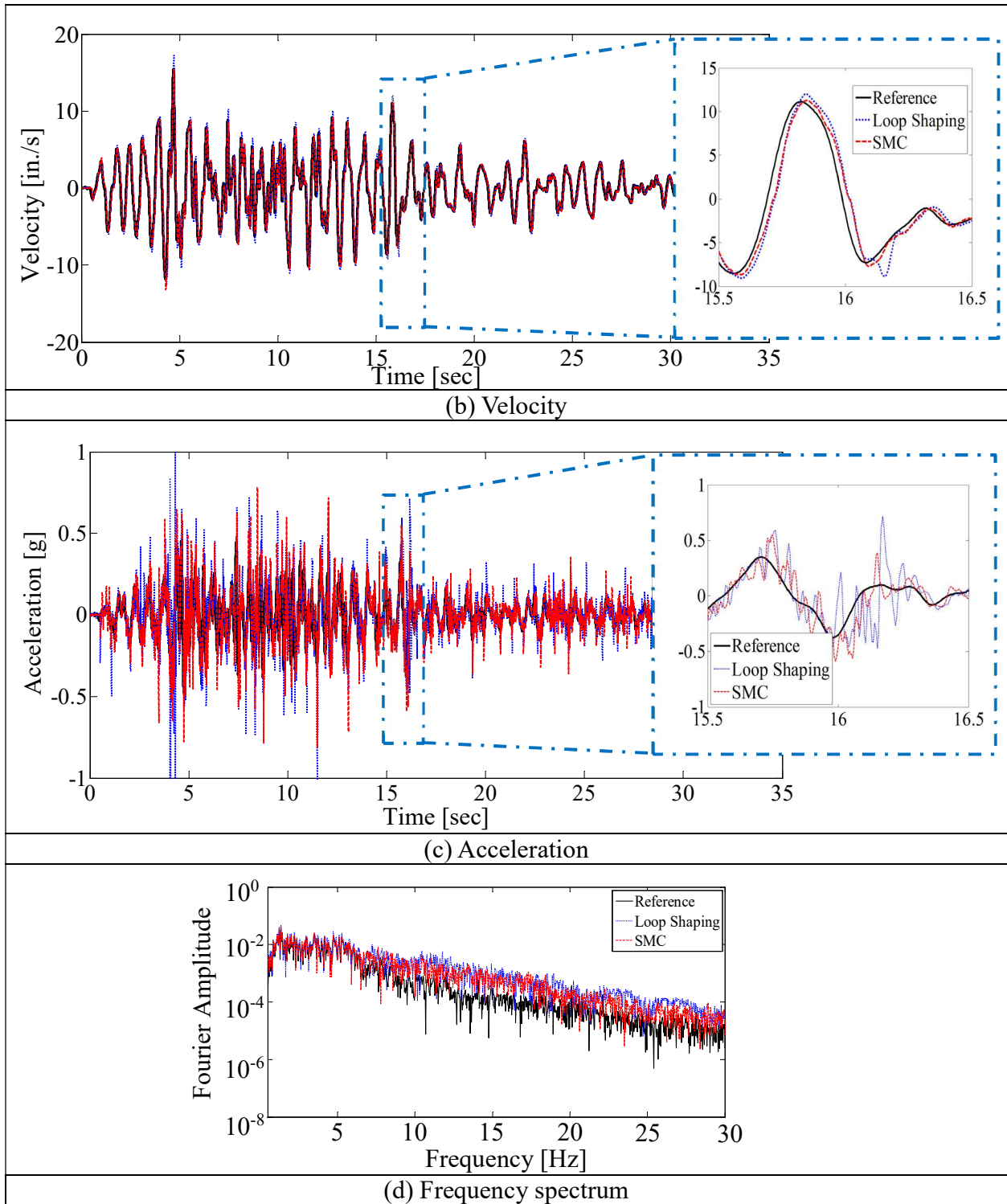


Figure 4-4 Comparison of the table performances

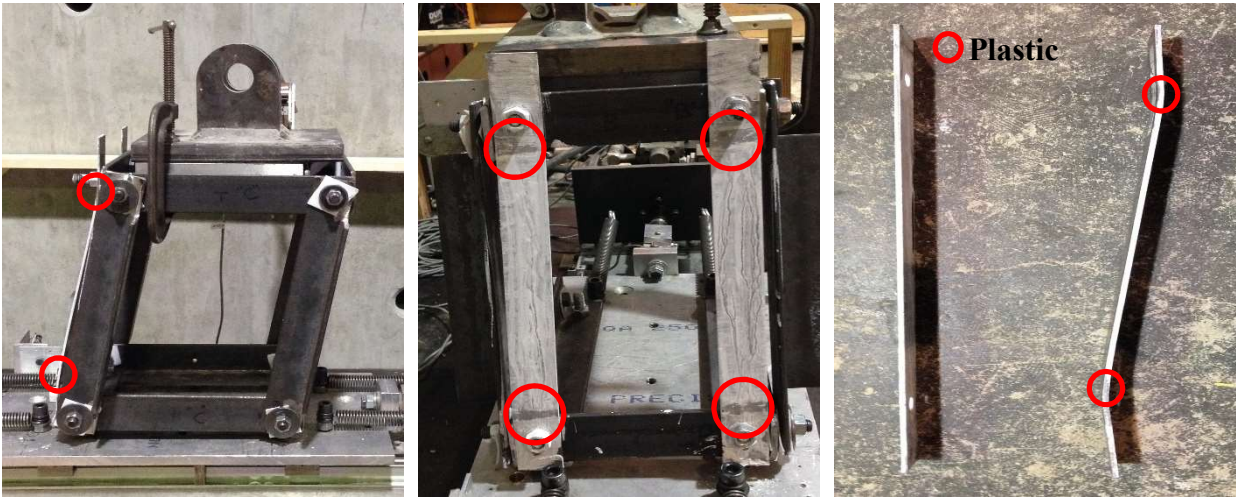


Figure 4-5 Photos of the damaged specimen

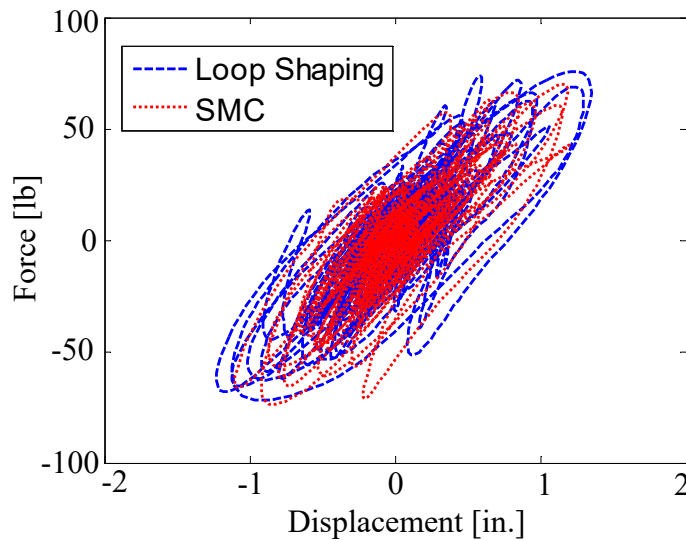


Figure 4-6 Specimen hysteresis

To confirm the effectiveness of the proposed hierarchical controller, seven additional earthquake time-history records are used to compare performances with the loop shaping displacement-based controller. Table 4-1 lists the root mean square of the error between the reference and measured table accelerations in the frequency and time domains. It should be noted that all errors are normalized against the maximum absolute value of the reference acceleration.

The results show that the the SMC can deal with the system nonlinearity and that it outperforms the loop shaping controller in both the time and frequency domains in terms of median and standard deviations.

Table 4-1 Acceleration tracking error analysis in time and frequency domains

Earthquake Name	Frequency domain [-]		Time domain [-]	
	Loop shaping	SMC	Loop shaping	SMC
Nahanni, Canada (1985)	0.51	0.50	7.68	6.86
Coalinga, USA (1983)	0.63	0.54	12.73	12.93
Kobe, Japan (1995)	0.44	0.39	17.43	15.19
Morgan Hill, USA (1984)	0.53	0.50	7.60	9.38
Northridge, USA (1994)	0.63	0.73	11.31	11.09
Irpinia, Italy (1980)	0.67	0.42	14.98	9.93
Manjil, Iran (1990)	1.49	1.06	20.59	20.23
Imperial Valley, US (1979)	2.21	1.61	13.64	10.31
Median	0.65	0.52	13.19	10.70
Standard Deviation	0.62	0.42	4.49	4.14

4.5 Summary

In this chapter, SMC is adopted as the high-level controller for reference signal tracking, and both the displacement-based and force-based linear controllers designed in Chapter 3 are employed as low-level controllers to regulate the hydraulic actuator to follow the command of the high-level controller. The real-time experiments were implemented on the scaled shake table at the University of British Columbia. Eight earthquake time-history records were used as reference signals. The experimental results show that the proposed hierarchical controller outperforms the single loop

shaping displacement-based controller designed in Chapter 3 when examining displacement, velocity and acceleration tracking. Although the individual low-level controller does not perform as well as the loop shaping controller, control allocation in the hierarchical framework with the SMC can compensate for such drawbacks in low-level controllers.

Chapter 5: Model Predictive Control

5.1 Overview

Model predictive control (MPC) originated in the late seventies and has developed considerably since then. The term “model predictive control” does not designate a specific control strategy. It essentially refers to a wide range of control methods which make explicit use of a model of the process to obtain the control signal by minimizing a cost function and obtain an optimal solution (Camacho, 2013). The various MPC algorithms only differ among themselves in the models used to represent the process and the noise and cost functions to be minimized.

The optimal control concept can be traced back to the work of Kalman in the 1960’s. Kalman developed a linear-quadratic regulator (LQR) to minimize a quadratic objective function (Kalman 1960b). The plant to be controlled can be described by the discrete-time, deterministic linear state-space model in Equation 5-1:

$$\begin{aligned}x_{k+1} &= Ax_k + Bu_k \\y_k &= Cx_k\end{aligned}\tag{Equation 5-1}$$

where vector u_k represents system input at time step k , vector x_k represents plant states at time step k and vector y_k represents plant output measurements at time step k .

The quadratic objective function to be minimized is defined in Equation 5-2. The squared input and state deviations are included, and the input weight matrices Q and R are introduced to allow for tuning trade-off.

$$J = \sum_{j=1}^{\infty} (\|x_{k+j}\|_Q^2 + \|u_{k+j}\|_R^2)$$

Equation 5-2

where the norm terms in the objective functions are defined in Equation 5-3:

$$\|x\|_Q^2 = x^T Q x$$

Equation 5-3

The optimal solution to the LQR problem was derived as a proportional control law with gain matrix K computed from the solution of a matrix Riccati equation:

$$u_k = -Kx_k$$

Equation 5-4

A dual state estimation theory termed Kalman Filter was developed to estimate the plant states from noisy input and output measurements (Kalman 1960a). The combination of LQR and Kalman Filter is called linear-quadratic-Gaussian (LQG) control, which provides a powerful solution to controlling linear system. Nevertheless, the constraints on the process inputs, states and outputs were not considered in the LQG control theory. Moreover, the process units to be controlled may have unique performance criteria that are difficult to address in the LQG control framework, which requires a time dependent weighting matrix, while the LQG control is not able to change the matrix content at every time step.

This issue advances the question of solving the dynamic optimization problem online at each control step. The control input sent to the plant serves to optimize future plant behaviour over a time interval known as the prediction horizon. The plant dynamics are described by the process model, while the plant input and output constraints are included directly in the objective function formulation, so that future constraint violations are considered and prevented. The first input of the optimal control input sequence is implemented into the plant, and the optimization problem is

solved again at the next time interval using the updated measurement data. This methodology is labelled model predictive control (Qin and Badgwell 2003).

Through the above literature review, the MPC has two main advantages compared to traditional linear control:

1. It can include the constraints for plant input and output to provide user flexibility in adjusting the safety bounds, which are based on the users' physical experiment's setup.
2. It can predict the optimal control sequence based on process model prediction rather than on blindly tuning for the parameters; thus, it can efficiently utilize the plant dynamics.

In this chapter, the MPC is employed as the high-level controller in the hierarchical control framework. The low-level control process is designed using the knowledge described in Chapters 2 and 3. The displacement, velocity and acceleration trajectory tracking are considered in the cost function design. The controller validation and performance investigation are done in the Simulink environment, which reveals the potential of the MPC in shake table control.

5.2 Theory

Figure 5-1 shows the MPC strategy and the basic idea behind the MPC are listed below as three steps.

1. Prediction: The future output for a determined horizon N , called the prediction horizon, are predicted at each time instant t using the process model. These predicted outputs $y(t+k|t)$, $k = 1 \dots N$ depend on the known values up to time instant t , which involve past inputs and outputs and the future control signals $u(t+k|t)$, $k = 0 \dots N-1$, which are those to be sent to the system and calculated based on the optimization result.
2. Optimization: The set of future control signals is calculated by optimizing a determined criterion to keep the process as close as possible to the reference trajectory $r(t+k)$. This

criterion usually takes the form of a quadratic function of the errors between the predicted output signal and the predicted reference trajectory. Essentially, in every single time instant, the MPC will solve a quadratic programming (QP) problem and calculate the optimal control sequence. This control sequence will be sent to the process model to provide a prediction for the system's behaviour.

3. Receding strategy: At each time instant t , only the control signal $u(t | t)$ is sent to the process while the other control signals calculated are rejected, since the next sampling instant $y(t + 1)$ is already known and Step 1 is repeated with this new value. All the sequences are brought up to date and the $u(t + 1 | t + 1)$ is re-calculated, which in principle will be different from the $u(t + 1 | t)$ because of the new measurement data available. The MPC is also called the receding horizon control (RHC) since, at each time instant t , the horizon is displaced towards the future, which involves the application of the first control signal of the sequence calculated at each time step.

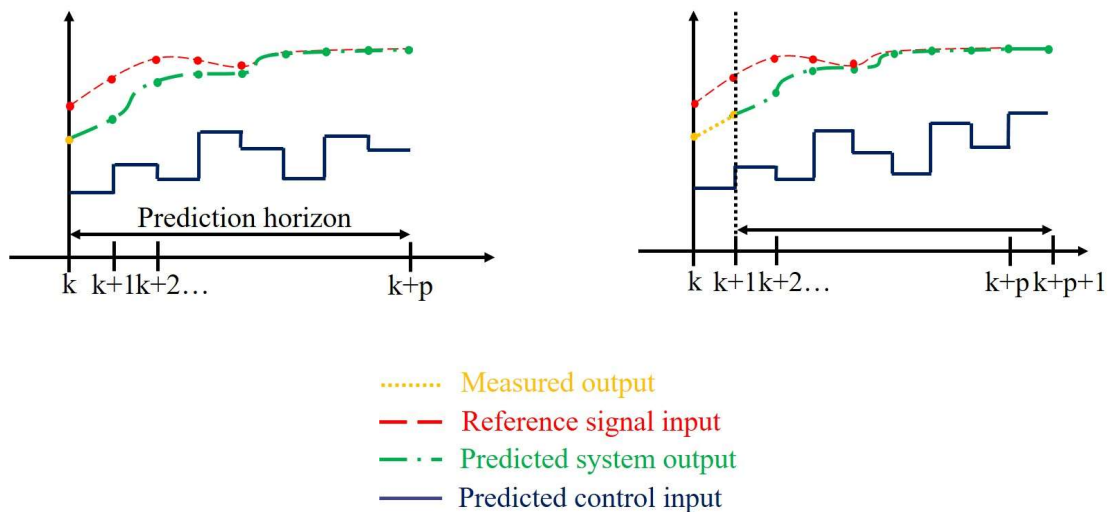


Figure 5-1 MPC schematic

In order to implement this strategy, the basic structure shown in Figure 5-2 is used. A process model is employed to predict the future plant output, based on past and current values and the proposed optimal future control sequence. These actions are calculated by minimizing the cost function, where the future tracking error and constraints are considered. The process model plays a decisive role in the controller. The chosen model must be able to capture the process dynamics to precisely predict the future output. Meanwhile, it is also required that it be simple enough to implement and understand.

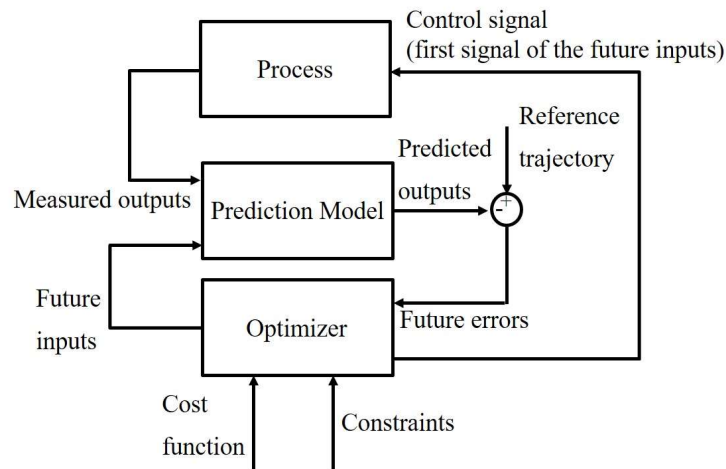


Figure 5-2 MPC structure

There are many types of models used in the various formulations. One of the most popular utilized in industry is the impulse response model. It is very simple to obtain since it only requires the measurement of the output when the process is excited with an impulse input. It is widely accepted in industrial practice because it is very intuitive and can also be used for multivariable processes. However, its main disadvantages are the large number of parameters needed and the fact that it can only describe open-loop stable processes. Similar to this model, the step response model can also be obtained when the input is a step.

The state space model is more widespread in the academic research community because of the simple way the controller can be derived even in multivariable cases. The state space description provides an easier expression of stability and robustness criteria. The transfer function model is also used in the academic research community. This type of model is better understood in industry than state space models, since some of the concepts used in the transfer function formula such as dead time, gains, and time constants are usually employed in industry.

Another fundamental part of the strategy is the optimizer. It provides control actions based on the process model and cost function. If the cost function is quadratic, its minimum can be obtained as an explicit function (linear) of past inputs and outputs and the future reference trajectory, which can significantly reduce computation effort. In the presence of inequality constraints, the solution must be obtained by more computationally numerical algorithms. The size of the optimization problems depends on the number of variables and the prediction horizons used. It should be noted that the amount of time needed for the constrained and robust cases can be various orders of magnitude higher than that needed for unconstrained cases, and that the bandwidth of the process to which the constrained MPC can be applied is considerably reduced.

5.3 Controller Design

The design of the MPC can be divided into the following three segments: the prediction model design, state estimation and prediction and optimization. This section will present the entire design procedure.

5.3.1 Prediction Model Design

To provide predictions of future plant behaviour, constructing the prediction model is the first step towards designing the MPC. Figure 5-3 outlines the prediction model architecture for the MPC. The prediction model can be separated into two parts: the process and disturbance models.

The process model aims at predicting the future behaviour of the control process, while the disturbance model is designed to solve the CSI effect mentioned in Chapter 2.

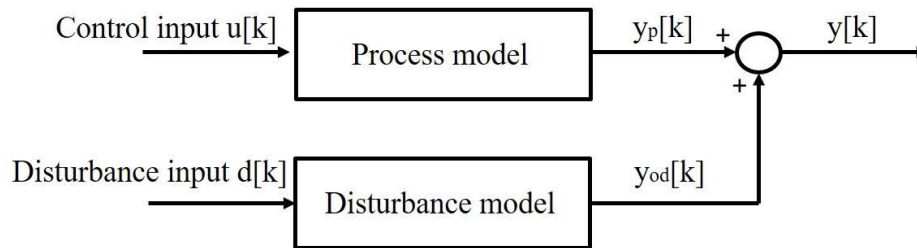


Figure 5-3 Prediction model architecture for MPC

It should be noted that the process model includes the TVC design mentioned in Chapter 3 and the hydraulic shake table model of Chapter 2. Figure 5-4 shows the process model block diagram for shake table applications. In other words, the process model here defines the entire low-level control process, rather than merely the dynamics of hydraulic actuators and shake tables.

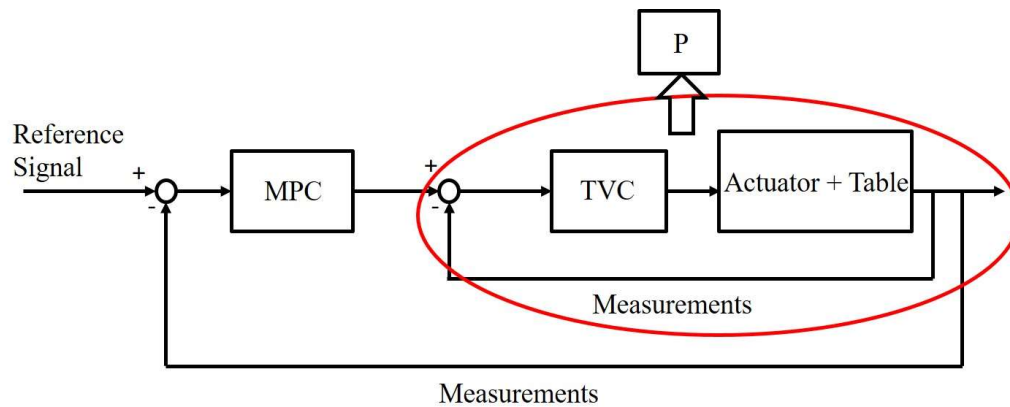


Figure 5-4 Process model block diagram

The modeling details for the hydraulic actuator and shake table are discussed in Chapter 2, while the TVC controller design is illustrated in Chapter 3. The overall low-level control process can be considered a control plant with three inputs and outputs including displacement, velocity and the acceleration control loop. The goal for the MPC is to calculate the optimized reference signal in displacement, velocity and acceleration for the low-level control process to track. Here,

the MPC uses a discretized model and a sampling frequency of 500 Hz. The process model is presented below in Equation 5-5.

$$\begin{aligned}
 x_p[k+1] &= A_p x_p[k] + B_p u[k] \\
 y_p[k] &= C_p x_p[k] + D_p u[k]
 \end{aligned}$$

$$A_p = \begin{bmatrix}
 1.003 & -0.004202 & -0.0008308 & -0.02242 & 0.000558 & 0.003639 \\
 0.1082 & 0.9194 & 0.2344 & -0.3925 & 0.01388 & 0.0636 \\
 0.1198 & -0.1882 & 0.9239 & -1.01 & 0.02332 & 0.164 \\
 0.03097 & -0.0001058 & -2.024 \cdot 10^{-5} & 0.9994 & 0.002001 & 3.673 \cdot 10^{-5} \\
 30.96 & -0.1263 & -0.0269 & -0.7197 & 1.004 & 0.05459 \\
 -3.325 \cdot 10^{-6} & 1.024 \cdot 10^{-8} & 1.841 \cdot 10^{-9} & -0.0003219 & -3.22 \cdot 10^{-7} & 1
 \end{bmatrix}$$

$$B_p = \begin{bmatrix}
 0.02311 & 0.0004731 & 3.639 \cdot 10^{-7} \\
 0.4039 & 0.008268 & 6.36 \cdot 10^{-6} \\
 1.041 & 0.02132 & 1.64 \cdot 10^{-5} \\
 0.0002333 & 4.775 \cdot 10^{-6} & 3.673 \cdot 10^{-9} \\
 0.3466 & 0.007097 & 5.459 \cdot 10^{-6} \\
 0.000322 & -3.865 \cdot 10^{-10} & -2.973 \cdot 10^{-13}
 \end{bmatrix}$$

$$C_p = \begin{bmatrix}
 0 & 0 & 0 & 1 & 0 & 0 \\
 0 & 0 & 0 & 0 & 1 & 0 \\
 1.551 \cdot 10^4 & -31.82 & -4.683 & -192.4 & -2.034 & 0
 \end{bmatrix}$$

$$D_p = \begin{bmatrix}
 0 & 0 & 0 \\
 0 & 0 & 0 \\
 0 & 0 & 0
 \end{bmatrix}$$

Equation 5-5

The first three states in Equation 5-5 are those of the hydraulic system model represented in Equation 2-11. The fourth and fifth states are the displacement and velocity of the shake table, respectively. The last is the integrator state in the TVC.

For the disturbance model, since there are three outputs including displacement, velocity and the acceleration feedback in the process model, a third order state space model is used to formulate the possible disturbances in the control process. The disturbance model is presented in Equation 5-6.

$$x_d[k+1] = A_d x_d[k] + B_d d[k]$$

$$y_d[k] = C_d x_d[k] + D_d d[k]$$

$$A_d = \begin{bmatrix} 1 & 0 & 0 \\ 0 & 1 & 0 \\ 0 & 0 & 1 \end{bmatrix}$$

$$B_d = \begin{bmatrix} 0.002 & 0 & 0 \\ 0 & 0.002 & 0 \\ 0 & 0 & 0.008 \end{bmatrix}$$

$$C_d = \begin{bmatrix} 10^4 & 0 & 0 \\ 0 & 10^4 & 0 \\ 0 & 0 & 2.5 \cdot 10^4 \end{bmatrix}$$

$$D_d = \begin{bmatrix} 0 & 0 & 0 \\ 0 & 0 & 0 \\ 0 & 0 & 0 \end{bmatrix}$$

Equation 5-6

By combining Equation 5-5 and Equation 5-6, the entire prediction model can be constructed.

$$x_c[k+1] = Ax_c[k] + Bu_0[k], x_c^T = [x_p^T x_d^T]$$

$$y[k] = Cx_c[k] + Du_0[k], u_0^T = [u^T d^T]$$

$$A = \begin{bmatrix} A_p & 0 \\ 0 & A_d \end{bmatrix}$$

$$B = \begin{bmatrix} B_p & 0 \\ 0 & B_d \end{bmatrix}$$

$$C = \begin{bmatrix} C_p & C_d \end{bmatrix}$$

$$D = \begin{bmatrix} D_p & D_d \end{bmatrix} \quad \text{Equation 5-7}$$

Since some of the states in the prediction model are unmeasurable and must be estimated to complete the computations in the model prediction section, a state estimator is designed to obtain the values for the unmeasurable states and predict the future plant output based on Equation 5-7.

5.3.2 State Estimation and Prediction

A steady state Kalman filter is constructed to estimate the states in Equation 5-7. The Kalman filter is an optimal estimator design for state estimation (Kalman 1960a). The Kalman filter is a set of mathematical equations that can estimate the state of a process recursively and minimize the mean of the squared error. The original Kalman filter is an observer with time-varying gain; however, the gain itself is typically rapid at reaching a constant value. This fact makes the steady state Kalman filter a good alternative to simplifying the implementations and calculations. The first step to designing the steady state Kalman filter is to solve the discrete algebraic Ricatti equation to get the *a priori* estimate error covariance M in Equation 5-8. Next, the Kalman gain, which will be constant throughout the entire control process, can be calculated in Equation 5-9.

$$AMA^T - M + Q - AMC^T [R + CMC^T]^{-1} CMA^T = 0 \quad \text{Equation 5-8}$$

$$K = MC^T (CMC^T + R)^{-1} \quad \text{Equation 5-9}$$

where A and C are defined in Equation 5-7, Q is the process noise covariance matrix and R is the measurement noise covariance matrix.

With the known Kalman gain, the Kalman filter estimation can be applied; the steps are presented in Equation 5-10 and Equation 5-11. It should be noted that Equation 5-10 is termed the measurement update and Equation 5-11 the time update.

$$x_c[k|k] = x_c[k|k-1] + K(y_m - Cx_c[k|k-1] - Du) \quad \text{Equation 5-10}$$

$$x_c[k+1|k] = Ax_c[k|k] + B_u u[k] \quad \text{Equation 5-11}$$

where y_m is the measured output and $B_u = \begin{bmatrix} B_p \\ 0 \end{bmatrix}$.

By using the states obtained from the steady state Kalman filter, the MPC can make predictions for the output variable, solve the optimization problem and generate the optimal control sequence. The optimization segment is discussed in the following section. With the control sequence known, the output prediction is performed by Equation 5-12 and Equation 5-13:

$$x_c[k+i|k] = Ax_c[k+i-1|k] + B_u u[k+i-1|k], i = 2, 3, \dots, p \quad \text{Equation 5-12}$$

$$y[k+i|k] = Cx_c[k+i|k] \quad \text{Equation 5-13}$$

where p is the prediction horizon.

5.3.3 Optimization

The optimizer solves the QP problem in each time interval and generates the optimal control input sequence. The cost function can be categorized as three terms: output reference tracking, constraint violation and control input change rate. The cost function design is presented in Equation 5-14. After the computation process, the MPC will generate displacement, velocity and the acceleration input sequence; the length of the sequence is the prediction horizon. As shown in Equation 5-15, z_k is the control sequence calculated by the MPC at time Step k and p is the

prediction horizon. u_{disp} , u_{vel} and u_{acc} are the control signals for the displacement, velocity and acceleration loop in the TVC, respectively.

$$J(z_k) = J_y(z_k) + J_{\Delta u}(z_k) + J_\varepsilon(z_k) \quad \text{Equation 5-14}$$

$$z_k^T = [u(k|k)^T \ u(k+1|k)^T \ \dots \ u(k+p-1|k)^T]$$

$$u(k|k) = [u_{disp}(k|k) \ u_{vel}(k|k) \ u_{acc}(k|k)] \quad \text{Equation 5-15}$$

The first term of the cost function is the output reference tracking term. Since there are three control loop in TVC, the output reference tracking term puts weighting on the tracking performance of each control loop and it is presented in Equation 5-16. w_{disp} , w_{vel} and w_{acc} are the weighting for displacement, velocity and acceleration control loop, respectively. r_{disp} , r_{vel} and r_{acc} are the reference input for displacement, velocity and acceleration, respectively. y_{disp} , y_{vel} and y_{acc} are the predicted displacement, velocity and acceleration from the Kalman filter, respectively.

$$J_y(z_k) = \sum_{i=1}^p \{w_{disp}[r_{disp}(k+i|k) - y_{disp}(k+i|k)]^2 + w_{vel}[r_{vel}(k+i|k) - y_{vel}(k+i|k)]^2 + w_{acc}[r_{acc}(k+i|k) - y_{acc}(k+i|k)]^2\}$$

$$\text{Equation 5-16}$$

The control input change rate is considered since in most of the process control application, it is preferable to have small control movement to prevent the sudden change in the entire process. Equation 5-17 shows the control input change rate term and $w_{\Delta disp}$, $w_{\Delta vel}$ and $w_{\Delta acc}$ are the weighting for displacement, velocity and acceleration input change rate, respectively.

$$J_{\Delta u}(z_k) = \sum_{i=0}^{p-1} \{w_{\Delta disp}[u_{disp}(k+i|k) - u_{disp}(k+i-1|k)]^2 + w_{\Delta vel}[u_{vel}(k+i|k) - u_{vel}(k+i-1|k)]^2 + w_{\Delta acc}[u_{acc}(k+i|k) - u_{acc}(k+i-1|k)]^2\}$$

$$\text{Equation 5-17}$$

Considering the physical limitations in the laboratory, the constraints for the output are also established and, therefore, can provide safety protection for the experimental setup. The constraint violation term is presented in Equation 5-18. ε_k is the slack variable for constraint softening purposes and ρ_ε is the weighting for constraint violation.

$$J_\varepsilon(z_k) = \rho_\varepsilon \varepsilon_k^2 \quad \text{Equation 5-18}$$

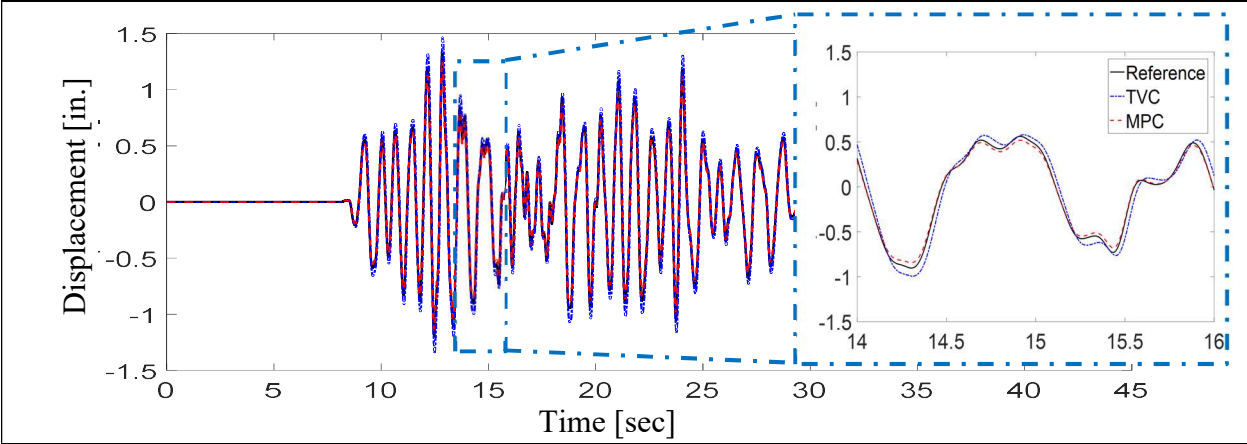
After the cost function is defined, the optimizer utilizes the KWIK algorithm (Schmid and Biegler 1994) to solve Equation 5-14 and ascertain the optimal control input sequence. The parameters in the MPC are presented in Table 5-1.

Table 5-1 MPC parameters setup

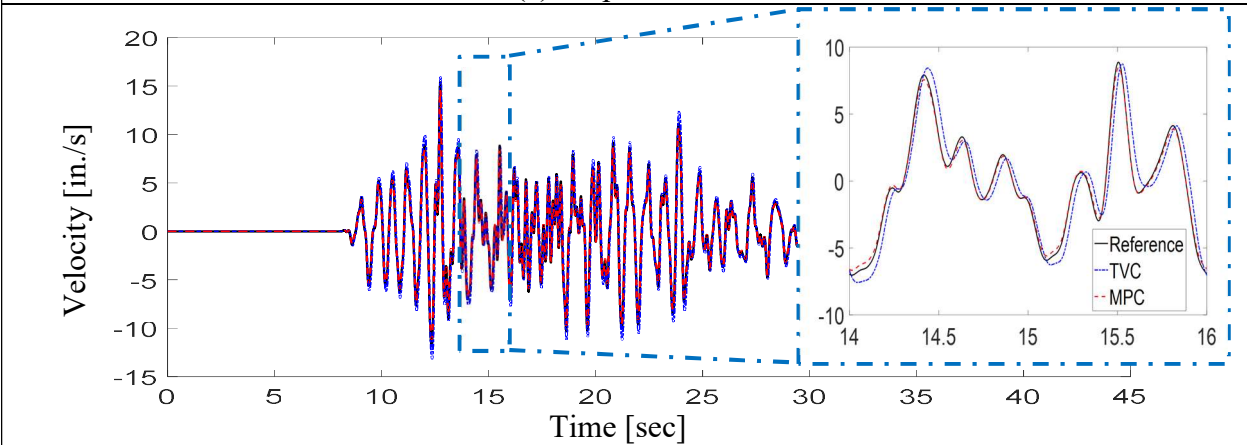
Prediction horizon	15
Weighting for output tracking [w_{disp} , w_{vel} , w_{acc}]	[5,3,1]
Weighting for control input change rate [$w_{\Delta disp}$, $w_{\Delta vel}$, $w_{\Delta acc}$]	[0.1,0.1,0.1]
Weighting for constraint violation ρ_ε	5000
Displacement output limitation	± 1.5 [inch]

5.4 Simulation Result

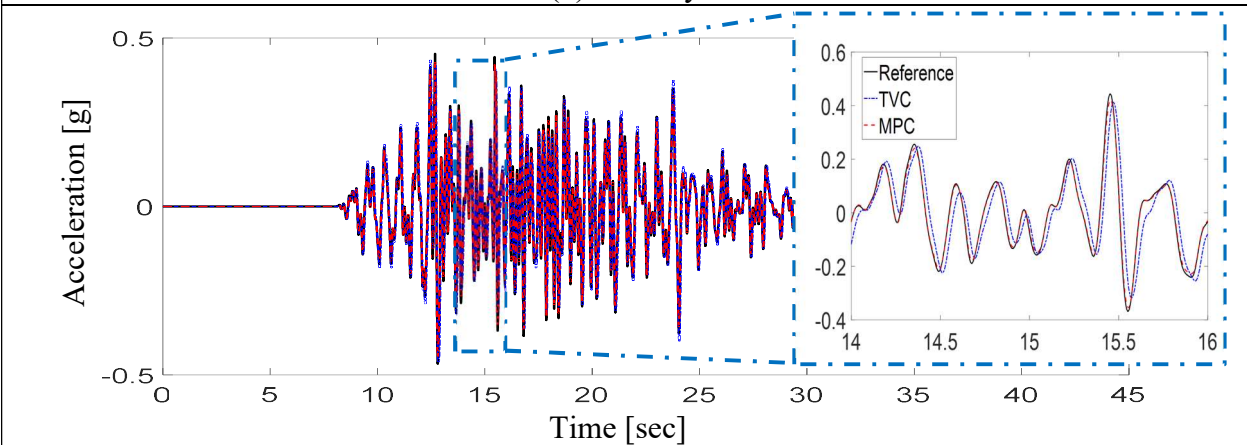
The MPC design and validation are implemented in the Simulink environment (Bemporad *et al.* 2010). The simulation results including the bare table conditions and specimen installed conditions are presented in this section. The 1980 Irpinia, Italy earthquake record is used as the reference signal. Figure 5-5 shows the comparison results for bare table simulation between the MPC and the TVC.



(a) Displacement



(b) Velocity



(c) Acceleration

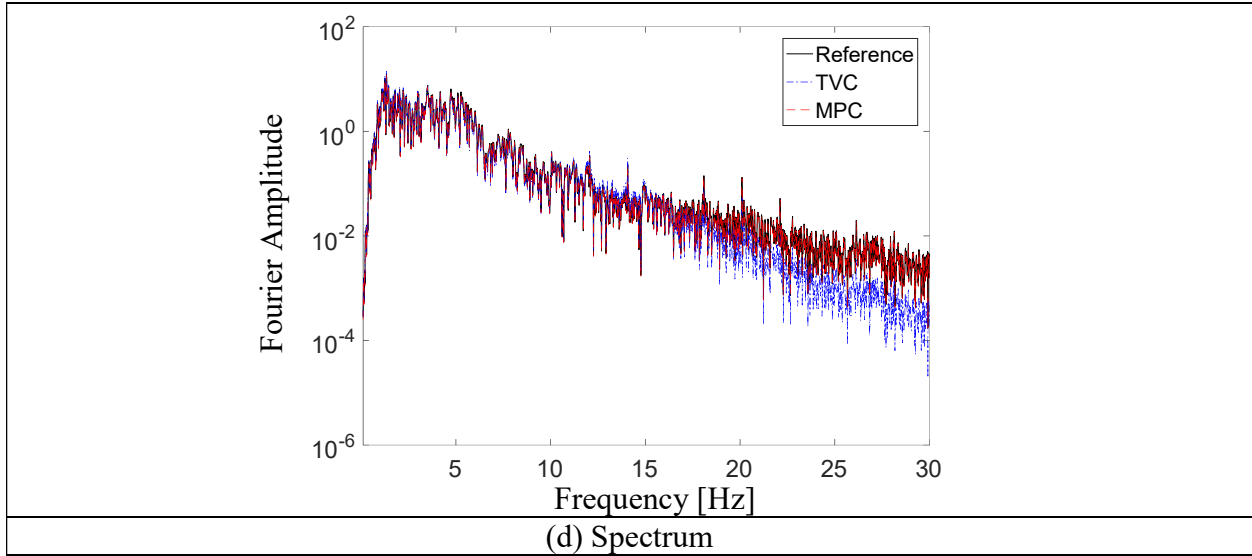
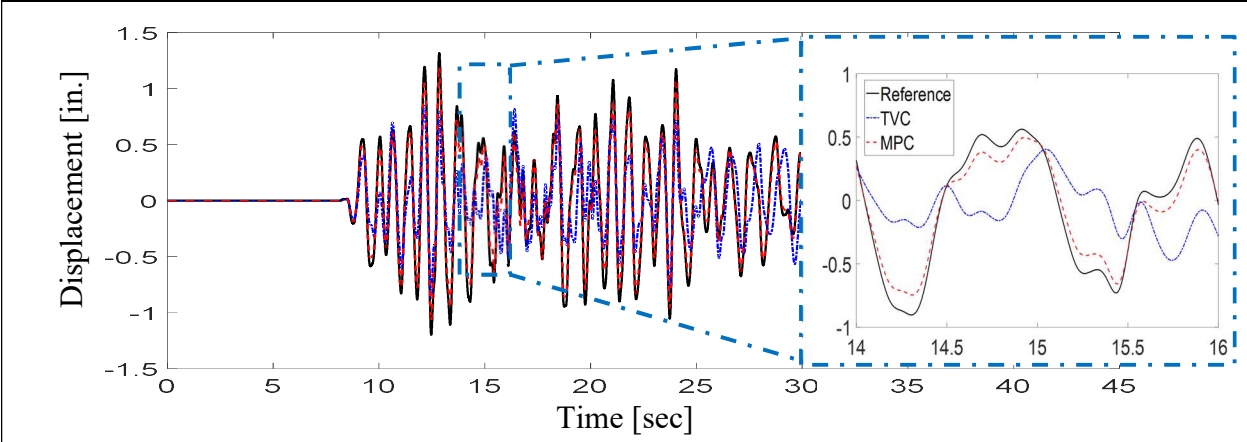


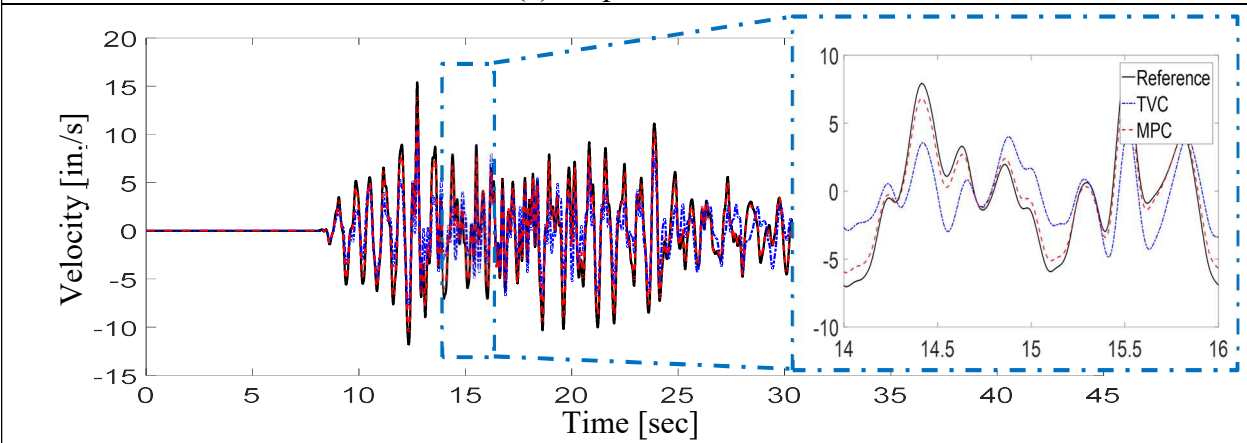
Figure 5-5 Comparison result for shake table without specimen

It can be observed that the phase response and tracking error are better in the MPC in time domain comparisons. Also, the frequency domain comparison reveals that the MPC has better tracking bandwidth and accuracy.

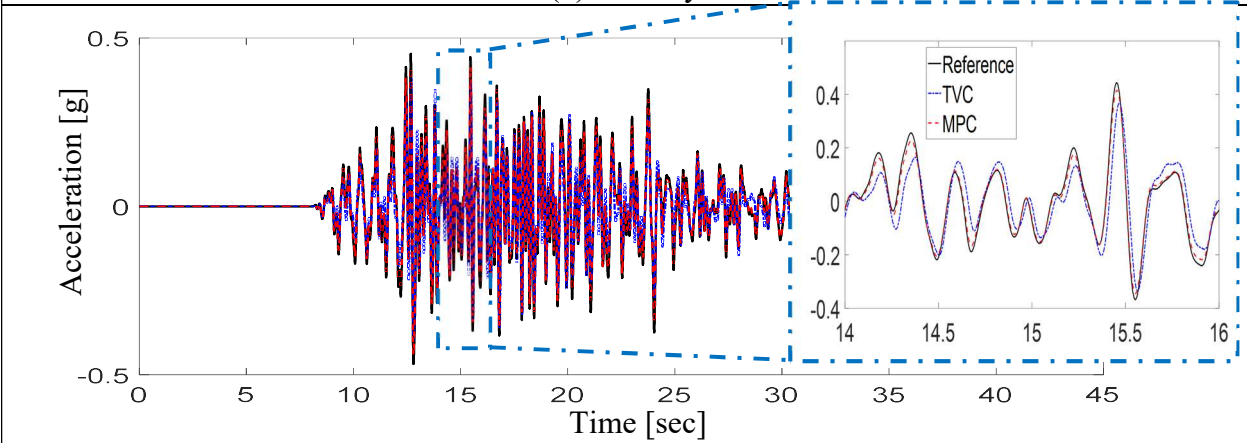
After validating the bare table simulation results, the linear specimen's condition is simulated to prove the robustness of the MPC. A 100 lbf. specimen with a 1 second structure period and 5% damping ratio is designed to provide specimen behaviour as a disturbance for the shake table control. The specimen design and equation of motion are discussed in Appendix A. Figure 5-6 shows the comparison results between the MPC and TVC for the specimen installed conditions.



(a) Displacement



(b) Velocity



(c) Acceleration

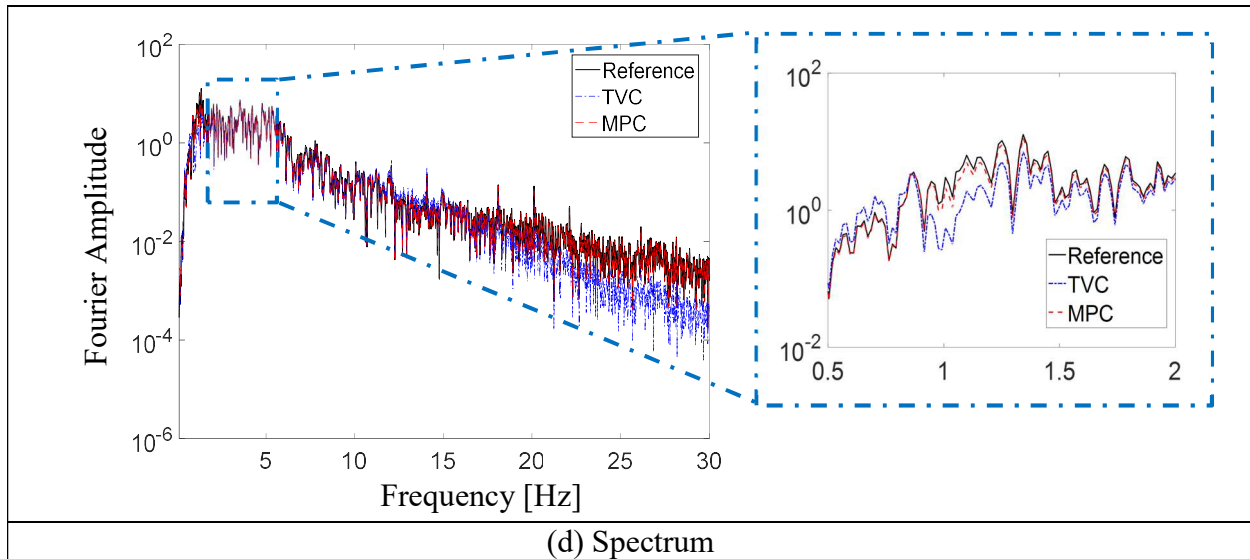


Figure 5-6 Comparison result for shake table with specimen

From the time domain results, it can be concluded that the TVC is influenced by the disturbance and that gain setup tuning is needed if the payload on the shake table has altered. However, the MPC can successfully achieve the disturbance rejection, while the time domain results reveal that the performance and robustness of the MPC are superior to that of the TVC. The frequency domain results illustrate that, since the specimen is installed and the structure period is 1 second, the tracking performance of the TVC was influenced in the low frequency area. However, the MPC can still achieve excellent tracking results in the frequency domain, which proves that the MPC has great potentiality in the industry to replace the existing linear controller design.

5.5 Comparison between SMC

Since the MPC and SMC are both high-level controllers in the hierarchical control framework, it is important to compare the pros and cons of these two controllers. Table 5-2 shows the acceleration tracking comparison for SMC and MPC. In both time domain and frequency domain, MPC has a better performance. Although MPC is still in simulation mode phase, the result

shows that MPC could potentially achieve better tracking performance than SMC in the real implementation.

Table 5-2 Acceleration tracking comparison for MPC and SMC

Earthquake Name	Frequency domain [-]		Time domain [-]	
	MPC	SMC	MPC	SMC
Nahanni, Canada (1985)	0.11	0.50	2.34	6.86
Coalinga, USA (1983)	0.24	0.54	5.99	12.93
Kobe, Japan (1995)	0.14	0.39	4.73	15.19
Morgan Hill, USA (1984)	0.15	0.50	4.79	9.38
Northridge, USA (1994)	0.10	0.73	3.22	11.09
Irpinia, Italy (1980)	0.23	0.42	7.05	9.93
Manjil, Iran (1990)	0.31	1.06	8.62	20.23
Imperial Valley, US (1979)	0.24	1.61	3.89	10.31
Median	0.19	0.52	4.76	10.70
Standard Deviation	0.08	0.42	2.06	4.14

The SMC utilizes the Lyapunov function and provides robustness to model uncertainties and nonlinearities, which is useful in shake table control. However, since its design lacks the information of the low-level control process, a command from the SMC may exceed the working range of the low-level controllers, potentially also contributing towards system instability.

In contrast, the design of the MPC includes a model of the entire low-level control process. Therefore, a command from the MPC will not exceed the capacity of the low-level controller. In the simulation mode, the MPC also demonstrates robustness and tracking performance under the

influence of specimen dynamics. Moreover, the limitations for the physical setup can also be considered in the MPC, which recommends this method for industrial purposes. However, since the model in this thesis is still linear, the tracking performance could be limited if the specimen is highly nonlinear. The nonlinear modeling technique should be investigated to improve the MPC performance.

5.6 Summary

In this chapter, the MPC is adopted as a high-level controller in the hierarchical control framework and then applied to the shake table control problem. In the low-level control stage, the simulation model built in Chapter 2 is used to provide hydraulic actuator dynamics in the prediction model. The TVC introduced in Chapter 3 is utilized as a low-level controller and provides the benchmark. The prediction model of the entire low-level control process is obtained by integrating the low-level controller and plant model and combining them with the disturbance model that was designed to solve the CSI effect issue. The state space model is presented in Section 5.3.1. Based on the estimation model, the MPC utilizes the steady state Kalman filter to conduct the state estimation and predict the control process's future behaviour. The cost function is defined in Section 5.3.3, while the weighting of the displacement, velocity, acceleration tracking and the changing rate of the control inputs are considered. The KWIK algorithm is used to solve the QP problem formulated in Section 5.3.3. The simulation results show that the MPC can successfully track the acceleration input signal, and that it provides sufficient robustness even the specimen dynamics is added to the simulation environment. This fact simply shows the potentiality of the MPC strategy in regulating hydraulic actuator dynamics and tracking the acceleration reference signal.

Chapter 6: Summary and Conclusion

6.1 Conclusion

Shake table control is a highly nonlinear control problem and in most of the existing research facilities, the linear control technique is applied to regulate the actuator and track the reference signal. Due to the existing nonlinearities in the hydraulic actuator, shake table and testing specimen, the traditional linear control method such as PID control cannot provide an universal solution to achieving the required performance for shake table control. The control-structure-interaction (CSI) effect changes the plant dynamics, making the employment of only one controller unrealistic for achieving good performance.

In this thesis, a novel hierarchical control framework has been introduced to solve this problem. A hierarchical control system is a form of control system in which a set of devices and governing algorithms is arranged in a hierarchical tree. The architecture consists of a high-level controller and one or more low-level controller(s). The advantage of the hierarchical control framework is that it can decompose the control problem into smaller sub-problems and then reassemble their solutions via a hierarchical tree. In this framework, high-level controller algorithms aim to regulate the overall structural dynamics, while low-level controllers focus on executing the commands from the high-level controller. The advantage of this framework is that it can simplify the control problem and provide a more efficient and effective solution. A scaled hydraulic shake table is constructed in the structure laboratory at the University of British Columbia to validate the concept illustrated in this thesis.

To develop a high-performance control strategy, obtaining the plant system's information is necessary. The hydraulic actuator dynamics is first investigated and, from the physical equation, the CSI effect can be well explained. It is critical to provide mathematical proof for tracking the performance and system stability in the controller design phase. Consequently, the system identification procedure is proposed to obtain a numerical model for the hydraulic shake table system. The grey box method is chosen to conduct the system identification, so the subspace system identification method is utilized to fit a precise model from the experimental data. The results of this conforming reveal that the numerical model can precisely capture the dynamics of the hydraulic shake table system. This method provides a positive approach to developing a control strategy and validating the control performance without implementing the real test in the laboratory; this can tremendously reduce costs.

Three control methods are introduced in the low-level controller design phase, including the proportional-integral-differential (PID) control, three-variable-control (TVC) and the loop-shaping control. The PID control is the algorithm most widely applied in industrial applications. It utilizes a combination of proportional, integral and derivative actions on the tracking error to generate the control output signal and send it the plant signal to minimize tracking error. It is already proven that the PID controller can successfully stabilize and regulate the hydraulic actuator; however, the control performance, including precision and bandwidth, are unable to meet the requirements for the shake table test. Therefore, the TVC has been developed to improve bandwidth control. Velocity and acceleration control loop are used to increase the bandwidth. Last, the state-of-the-art frequency domain design method labelled the loop-shaping control has been discussed. It makes use of the frequency response of the plant model and designs the controller to achieve the desired performance.

Two high-level controller examples are provided to solve the existing problems in the shake table test; these include the sliding mode control (SMC) and model predictive control (MPC). The SMC is a suitable solution to system uncertainties and the nonlinear control problem. It follows the Lyapunov theorem and provides robustness for handling nonlinearities. Experimental work was conducted on the scaled hydraulic shake table in the structure laboratory at the University of British Columbia to validate the feasibility of the SMC. The experimental results show that the SMC can compensate for the insufficient portions of the low-level controller and provide good tracking results for nonlinear specimen behaviour.

On the other hand, the MPC follows a model-based approach and utilizes the plant model to solve the QP optimization problem at each time step. In the MPC design, the Kalman filter is used for state estimation and prediction of the low-level control process, and the cost function includes the tracking error in the displacement, velocity and acceleration control mode for the optimization purpose. In the simulation phase, the MPC demonstrates a high level of accuracy and robustness under specimen behaviour and should thus be considered a potential candidate for real-time shake table control.

In summary, the concepts and challenging problems of hydraulic shake table control have been well explained in this thesis. The hierarchical control strategy was developed to improve control performance. The system identification procedure was performed to obtain a reliable simulation model of the hydraulic actuator and shake table. Diverse control methods were presented at both the low-level and high-level control phases and the hierarchical control strategy was proven to be a feasible method for the hydraulic shake table control problem. More advanced control algorithms can be implemented under this architecture.

6.2 Future Work

The following future work was planned based on the contents and control architecture illustrated in this thesis.

1. The MPC has already been proven in the simulation phase as providing good tracking performance. Real-time control implementation should be conducted to further investigate the method's tracking performance and robustness. Following real-time implementation, a more advanced version of the MPC can be further studied. For instance, the adaptive MPC could be a possible solution since it was shown to update the plant model, while the normal MPC simply used a consistent model throughout the experiment.
2. In the system identification phase, the model for this thesis was still linear; this might not fully describe the system's characteristics in diverse scenarios. A nonlinear modeling technique such as a neural network or machine learning method might be further studied to generate a precise, nonlinear model for the hydraulic shake table system.
3. There still remain for study various modified versions of the sliding model control, such as the multiple sliding surface control (MSSC), dynamic surface control (DSC) and receding horizon sliding control (RHSC). The MSC and DSC have different manners for the sliding surface design, while the RHSC is actually a combination of the MPC and SMC. They all have the potentiality to outperform the existing version of SMC.
4. After the SDOF shake table control system is fully studied, the control object should be extended to the multiple degrees of freedom (MDOF) shake table control

system.

5. The experience of controller development in shake table tests should also be applicable to structure control. Both semi-active and active controls require hydraulic actuator control, system identification procedure and advanced control algorithm design, which are also challenging issues.

Bibliography

- Bemporad, Alberto, Manfred Morari, and N. Lawrence Ricker. 2010. *Model Predictive Control Toolbox User's Guide*. The Mathworks.
- Bennett, Stuart. 1993. "Development of the PID Controller." *IEEE Control Systems* 13 (6): 58–62.
- Camacho, E. F., and C.B. Alba. 2013. *Model Predictive Control*. Springer Science & Business Media. doi:10.1007/978-0-85729-398-5.
- Dyke, S. J., B. F. Spencer, P. Quast, and M. K. Sain. 1995. "Role of Control-Structure Interaction in Protective System Design." *Journal of Engineering Mechanics* 121 (2): 322–38.
- Garnier, H., M. Mensler, and A. Richard. 2003. "Continuous-Time Model Identification from Sampled Data: Implementation Issues and Performance Evaluation." *International Journal of Control* 76 (March 2015): 1337–57. doi:10.1080/0020717031000149636.
- Jean-Jacques E. Slotine, and Weiping Li. 1991. *Applied Nonlinear Control*. Englewood Cliff, New Jersey, Prentice-Hall Inc.
- Jelali, Mohieddine, and Andreas Kroll. 2012. *Hydraulic Servo-Systems: Modelling, Identification and Control*. Springer Science & Business Media.
- Kalman, R. E. 1960a. "A New Approach to Linear Filtering and Prediction Problems." *Journal of Basic Engineering* 82 (1): 35. doi:10.1115/1.3662552.
- . 1960b. "Contributions to the Theory of Optimal Control." *Boletín de La Sociedad Matemática Mexicana* 5 (2): 102–19. doi:10.1016/0016-0032(63)90689-6.
- Ljung, Lennart. 1999. *System Identification: Theory for User 2nd Edition*. PTR Prentice Hall Upper Saddle River NJ.
- . 2009. "Experiments with Identification of Continuous Time Models." *IFAC Proceedings*

- Volumes (IFAC-PapersOnline)* 15 (PART 1): 1175–80. doi:10.3182/20090706-3-FR-2004.0209.
- McFarlane, D., and K.Glover. 1992. “A Loop-Shaping Design Procedure Using H-Infinity Synthesis.” *IEEE Transactions on Automatic Control* 37 (6): 759–69. doi:10.1109/9.256330.
- Nakata, Narutoshi. 2010. “Acceleration Trajectory Tracking Control for Earthquake Simulators.” *Engineering Structures* 32 (8). Elsevier Ltd: 2229–36. doi:10.1016/j.engstruct.2010.03.025.
- Nowak, Richard F, David AKusner, Rodney LLarson, and Bradford KThoen. 2000. “Utilizing Modern Digital Signal Processing for Improvement of Large Scale Shaking Table Performance.” In *12th World Conference on Earthquake Engineering*.
- Overchee, V., and B. L.Moor. 1996. *Subspace Identification For Linear Systems*.
- Ozcelik, Ozgur. 2008. “A Mechanics-Based Virtual Model of NEES-UCSD Shake Table: Theoretical Development and Experimental Validation.” *ProQuest*. <http://escholarship.org/uc/item/9tt3b67n>.
- Phillips, Brian M., Nicholas E.Wierschem, and B. F.Spencer Jr. 2014. “Model-Based Multi-Metric Control of Uniaxial Shake Tables.” *Earthquake Engineering and Structure Dynamics* 43 (5): 681–99. doi:10.1002/eqe.
- Qin, S. Joe, and Thomas A.Badgwell. 2003. “A Survey of Industrial Model Predictive Control Technology.” *Control Engineering Practice* 11 (7): 733–64.
- Schmid, C., and L. T.Biegler. 1994. “Quadratic Programming Hessian.” *Computers & Chemical Engineering* 18 (9): 817–32.
- Severn, R. T. 2011. “The Development of Shaking tables—A Historical Note.” *Earthquake Engineering and Structure Dynamics* 40 (June 2010): 195–213. doi:10.1002/eqe.1015.
- Stehman, Matthew, and Narutoshi Nakata. 2013. “Direct Acceleration Feedback Control of Shake

- Tables with Force Stabilization.” *Journal of Earthquake Engineering* 17 (5): 736–49.
doi:10.1080/13632469.2013.776508.
- Tagawa, Y., and K.Kajiwara. 2007. “Controller Development for the E-Defense Shaking Table.” *Proceedings of the Institution of Mechanical Engineers, Part I: Journal of Systems and Control Engineering* 221 (2): 171–81. doi:10.1243/09596518JSCE331.
- Utkin, V. 1977. “Variable Structure Systems with Sliding Modes.” *IEEE Transactions on Automatic Control* 22 (2): 212–22. doi:10.1109/TAC.1977.1101446.
- Wright, Stephen, and Jorge Nocedal. 1999. *Numerical Optimization*. Springer Science 35.
doi:10.1007/BF01068601.
- Yao, J., M.Dietz, R.Xiao, H.Yu, T.Wang, and D.Yue. 2014. “An Overview of Control Schemes for Hydraulic Shaking Tables.” *Journal of Vibration and Control*, no. July 2014: 1–17.
doi:10.1177/1077546314549589.

Appendices

Appendix A Simulation specimen design

This section introduces the simulation model design of the linear specimen and the equation of motion for the SDOF shake table including specimen. Figure A-1 shows the schematic diagram of the SDOF shake table model.

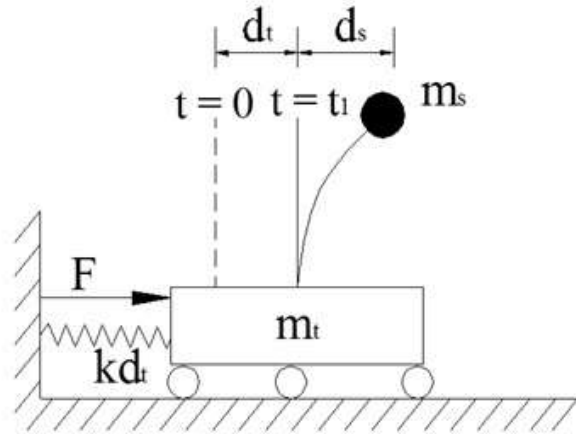


Figure A-1 Schematic Diagram of the SDOF Shake Table Model

The equation of motion for this system can be listed in Equation A-1 and Equation A-2:

$$m_s(\ddot{d}_t + \ddot{d}_s) + c_s \dot{d}_s + k_s d_s = 0 \quad \text{Equation A-1}$$

$$m_t \ddot{d}_t + c_t \dot{d}_t + k_{d_t} d_t - c_s \dot{d}_s - k_s d_s - F = 0, \quad \text{Equation A-2}$$

where m_t and m_s are the mass for the shake table and specimen, respectively; c_t and c_s are the damping coefficient for the shake table and specimen, respectively; and k_s are the stiffness for the shake table and specimen, respectively.

Transforming Equation A-1 and Equation A-2 into a state space representation, Equation A-3 can be derived as follows:

$$\begin{Bmatrix} x_1 \\ x_2 \\ x_3 \\ x_4 \end{Bmatrix} = \begin{Bmatrix} d_t \\ \dot{d}_t \\ d_s \\ \dot{d}_s \end{Bmatrix}$$

$$\begin{Bmatrix} \dot{x}_1 \\ \dot{x}_2 \\ \dot{x}_3 \\ \dot{x}_4 \end{Bmatrix} = \begin{Bmatrix} x_2 \\ \frac{1}{m_t}(k_s x_3 + c_s x_4 + F - kx_1 - c_t x_2) \\ x_4 \\ -\frac{1}{m_t}(k_s x_3 + c_s x_4 + F - kx_1 - c_t x_2) - \frac{1}{m_s}(k_s x_3 + c_s x_4) \end{Bmatrix}$$

Equation A-3

Equation A-3 can be further converted into a matrix form in Equation A-4. The input of the system is the force from the hydraulic actuator, while the output is the displacement, velocity and acceleration of the shake table.

$$\dot{x} = Ax + Bu$$

$$y = Cx + Du ,$$

$$A = \begin{bmatrix} 0 & 1 & 0 & 0 \\ \frac{k}{m_t} & \frac{c_t}{m_t} & \frac{k_s}{m_t} & \frac{c_s}{m_t} \\ 0 & 0 & 0 & 1 \\ \frac{k}{m_t} & \frac{c_t}{m_t} & \left(-\frac{k_s}{m_t} \frac{k_s}{m_s}\right) & \left(-\frac{c_s}{m_t} \frac{c_s}{m_s}\right) \end{bmatrix}$$

$$B = \begin{bmatrix} 0 \\ \frac{1}{m_t} \\ 0 \\ \frac{1}{m_t} \end{bmatrix}$$

$$C = \begin{bmatrix} 1 & 0 & 0 & 0 \\ 0 & 1 & 0 & 0 \\ \frac{k}{m_t} & \frac{c_t}{m_t} & \left(-\frac{k_s}{m_t} \frac{k_s}{m_s}\right) & \left(-\frac{c_s}{m_t} - \frac{c_s}{m_s}\right) \end{bmatrix}$$

$$D = \begin{bmatrix} 0 \\ 0 \\ \frac{1}{m_t} \end{bmatrix}$$

Equation A-4

Comparing Equation 2-5 and Equation 2-28, the parameters of the shake table can be obtained. The specimen is designed using 100 lbf. as the weight, 1 second as the structure period and 5% as the damping ratio. The Matlab code to calculate the matrix content in Equation A-4 is attached below. By using the generated state space model, the SDOF shake table with its specimen installed can be simulated in the Simulink environment.

Matlab code:

```
% shake table and specimen parameters
% unit for length is inch and unit for force is lb
mt = 0.1212; kt = 23.3189; ct = 0.2465; T = 1;
ms = 100/386.4; ks = ms*4*pi^2/(T)^2; cs = 2*0.05*ms*2*pi;

%%%%%%%%%%%%%%%%%%%%%%%%%%%%%%%%%%%%%%%%%%%%%%%%%%%%%%%%%%%%%%%%%%%%%%%%
% Matrix content
TA = [0 1 0 0;
      -(kt/mt) -(ct/mt) (ks/mt) (cs/mt);
      0 0 0 1;
      kt/mt ct/mt (-ks/mt - ks/ms) -cs/mt-cs/ms]
TB = [0;
      1/mt;
      0;
      -1/mt]
TC = [1 0 0 0;
      0 1 0 0;
      -(kt/mt) -(ct/mt) (ks/mt) (cs/mt);]
TD = [0;
      0;
      1/mt]
%%%%%%%%%%%%%%%%%%%%%%%%%%%%%%%%%%%%%%%%%%%%%%%%%%%%%%%%%%%%%%%%%%%%%%%%
```